Rocha, J.; Sena-Cruz, J.; Pereira, E. (2022) "Tensile behaviour of CFRP-glass adhesively bonded connections: double-lap joint tests and numerical modelling." Engineering Structures, 260: 114212, 21 pp.

TENSILE BEHAVIOUR OF CFRP-GLASS ADHESIVELY BONDED CONNECTIONS: DOUBLE-LAP JOINT TESTS AND NUMERICAL MODELLING

Jorge Rocha[1], José Sena-Cruz[2], Eduardo Pereira[3]

ABSTRACT: Within the context of glass structures, reinforcement strategies have been recently developed to prevent catastrophic failures by promoting the composite action between components. In this regard, the behaviour of adhesively bonded connections between glass and the reinforcement plays a crucial role. This paper presents an experimental, analytical and numerical study focussing on the bond behaviour of CFRP-to-glass adhesively bonded joints, comprising annealed glass sheets and CFRP laminates bonded with two stiff adhesives and one flexible adhesive. The experimental programme included (i) mechanical characterization tests and (i) tensile tests on CFRP-to-glass double-lap joints, evaluating the influence of the type of adhesive and the overlap length. Digital image correlation (DIC) method, analytical investigations and numerical modelling were performed to determine the local bond stress-slip laws for each adhesive, aiming at providing the required information to subsequently support the design of glass structural elements. Compared to the flexible adhesive, the stiff adhesives seem to promote more favourable interaction between the adherends; however, the former is better at promoting stress redistribution mechanisms, therefore, mobilizing longer bond lengths to transfer the tensile force between adherends. Adhesives with an extremely stiff response induce high stress concentrations in small areas and, consequently, the bonding system may fail prematurely at the glass adherend governed by localized phenomena, such as the low quality of glass processing methods, the high density of surfaces flaws and localized damage during handling.

[1] PhD Student, ISISE, IB-S, University of Minho, School of Engineering, Campus de Azurém, 4800-058 Guimarães, Portugal. Email: a61858@alunos.uminho.pt

[2] Associate Professor, ISISE, IB-S, University of Minho, School of Engineering, Campus de Azurém, 4800-058 Guimarães, Portugal. Email: jsena@civil.uminho.pt

[3] Assistant Professor, ISISE, IB-S, University of Minho, School of Engineering, Campus de Azurém, 4800-058 Guimarães, Portugal. Email: eduardo.pereira@civil.uminho.pt

KEYWORDS: Annealed glass; CFRP composite materials; Stiff and flexible adhesives; Bond behaviour; Analytical model; Numerical simulations;

1. INTRODUCTION

In recent years, structural glass has gained great relevance in contemporary architecture due to its aesthetic possibilities and transparency [1,2]. However, the structural behaviour of glass is substantially different from other traditional building materials, such as steel and reinforced concrete [3], requiring the adoption of appropriate safety measures to prevent catastrophic collapses due to its brittle behaviour. These safety measures must ensure that the failure of any structural element does not cause the unexpected collapse of the entire structure (fail-safe), ensuring an adequate load carrying capacity to allow the evacuation of people or, if possible, to proceed to the replacement of the damaged element [4].

With the aim of improving the structural performance of annealed glass, the industry has also developed glass toughening to increase its tensile strength, and glass lamination to overcome its brittleness [1,4]. In the first technique, the glass is subjected to thermal treatment, called "tempering", which creates compressive stresses on its surfaces and surroundings, closing flaws and, therefore, increasing its tensile strength. However, the tempering effect leads to undesirable features for structural applications, since the breakage of tempered glass creates smaller fragments, which reduces the residual strength [1,2,4]. Glass lamination is based on joining two or more sheets of glass by means of a polymeric interlayer. Therefore, the lamination method is based on structural redundancy. If one glass sheet breaks, the additional sheets will prevent the failure of the entire element and the fragments will remain in place due to the interlayer action. However, the brittle behaviour of glass is also not eliminated by this method.

Therefore, several safety approaches have been studied recently to mitigate the brittle behaviour of glass through the composite action between glass and an integrated reinforcement material, namely the glass hybrid systems with timber (e.g. [5,6]), stainless steel (e.g. [7–10]), Carbon Fibre Reinforcement Polymers – CFRP (e.g. [11,12]) and Glass Fibre Reinforcement Polymers – GFRP (e.g. [1,2,13–15]). This concept, somewhat similar to the one found in reinforced concrete or composite construction systems, provides residual strength and stiffness after glass cracking by promoting the transfer of tensile stresses from the glass to the reinforcement through the intermediary adhesive layer [2]. Although some of the reinforcements used have a brittle behaviour, such as glass, the sequential failure of these materials and/or connections allows the glass hybrid systems to exhibit non-linear inelastic behaviour, with progressive decrease in stiffness with increasing load [16]. This behaviour is commonly designated as pseudo-ductility because it can only develop at the system level.

The composite action between glass and reinforcement, materialized by an adhesive joint, is crucial for the structural behaviour of composite glass systems. Thus, for composite elements it is particularly important to determine the mechanical properties of the adhesives used and the structural behaviour of joints under loading, with respect to the substrate materials, the thickness of the adhesive layer, the effect of environmental conditions and the duration and rate of the load [17]. Some studies are found addressing the bond behaviour of glass hybrid systems. Steel-to-glass (e.g. [17–19]) and GFRP-to-glass (e.g. [2,20]) connections have been investigated recently, using different types of adhesive to assess their influence on the shear interaction between adherends. Moreover, the interlayer has also been studied as a bonding agent when the reinforcement is introduced within the laminated glass panel before the lamination process (e.g. [18]). Different test setups have been adopted, such as single lap joint tests (e.g. [19]), double-lap joint tests (e.g. [2]) and pull-out tests (e.g. [18]). Most studies have focused on the experimental assessment of the composite action of glass hybrid systems. Additional studies are required to accurately characterize such composite systems, namely towards the development of reliable design tools, whether analytical (e.g. [20]) or numerical (e.g. [21]).

Few studies have been addressing the bond behaviour of glass hybrid systems, and the experimental research in this topic has been mostly dedicated to the flexural behaviour of steel reinforced (e.g. [7–10]) and GFRP reinforced glass composite systems (e.g. [1,2,13–15]). Although CFRP materials are widely used in the construction industry (e.g. strengthening of existing concrete structures), only a limited number of studies have focused on the behaviour of CFRP-glass composite systems (e.g. [11,12]). Furthermore, to the best of the authors' knowledge, there are no studies in the literature related to the bond behaviour of CFRP-to-glass connections. Therefore, this research is important to support the future development of design guidelines and approaches for glass reinforced structures.

Given the lack of studies focusing on the composite action and on the flexural behaviour of CFRP-glass composite systems, this research aimed to study these systems at the level of the adhesive joint, based on an experimental and analytical/numerical research on CFRP-to-glass adhesively bonded joints. The experimental programme included the mechanical characterization tests of the different materials and the tensile testing of double-lap joints. Three different adhesives were selected taking into account the technical specifications provided by the suppliers, in order to assess the influence of the adhesive's nature on the behaviour of the CFRP-glass connections. In addition, the Digital Image Correlation (DIC) method was used to support the analysis of the results obtained from double-lap joint tests, capturing the propagation of adhesive damage with increasing load, as well as the stress concentration near the loaded end section [22]. DIC processing was performed by using the

GOM Correlate 2019 software [23]. The second part of this paper presents the analytical/numerical studies considering the double-lap joint test results obtained. The analytical studies were based on solving the 2nd order equation of bond, while for the numerical studies ABAQUS commercial package v6.14 [24] was used.

2. MATERIALS AND METHODS

As stated in the introductory section, this work includes an experimental investigation on the bond behaviour of CFRP-to-glass adhesively bonded joints using adhesives of different stiffness. The study comprised (i) the characterization of the involved materials and (ii) tensile tests on double-lap joint specimens. The material characterization tests provided the mechanical properties of the CFRP laminates and the adhesives used, namely their tensile modulus of elasticity and corresponding tensile strength. On the other hand, the double-lap joint tests allowed comparing the performance of the different adhesives in terms of (i) their feasibility to be used as bond agent in structural glass joints and (ii) their influence on the structural behaviour of CFRP-to-glass connections, namely the overall response, stiffness and strength. This section summarizes the experimental procedures adopted in both tests.

2.1. Materials characterization

The CFRP laminates used in the experimental campaign, with a cross section of 50 × 1.2 [mm], were produced by S&P® Clever Reinforcement Company. These laminates are composed of unidirectional carbon fibres agglutinated with an epoxy vinyl ester resin matrix, presenting a smooth surface and a fibre fraction of about 70% in volume. The mechanical properties of the CFRP laminates have been characterized according to ISO 527-5:2009 [25]. Thus, samples of 250 × 50 × 1.2 [mm] (length × width × thickness) were extracted. Metallic tabs of 50 mm length were glued to the ends to avoid premature failure of the specimens due to stress concentrations introduced by the griping system of the testing machine. A clip gauge (type: MFA 12; linearity: 0.1 %; sensitivity: 2.0 mV/V; resolution: 1.0 pm; precision: ±1.5 μm) with 50 mm of gage length was placed at the central region of each specimen to allow assessing the modulus of elasticity (E_{CFRP}), which was determined from the linear portion of the stress-strain response between strain values of 0.05 % and 0.25 % [25].

The adhesives for bonding the reinforcement to the glass were selected based on the literature on hybrid glass systems and taking into account their technical characteristics and the materials to be joined (glass and CFRP). In addition, these adhesives showed different stiffness in order to allow the assessment of its influence on the structural behaviour of composite CFRP-glass systems. Therefore, to cover the wide range of commercial adhesives suitable for CFRP-glass connections, three adhesives were tested: (i) the two-component polyurethane adhesive SikaForce®-7710 L100 [26], with low modulus of elasticity; (ii) the two-component epoxy resin-based adhesive SikaDur®-330 [27], with high modulus of elasticity; and the two-component epoxy resin-based adhesive 3M Scotch-Weld DP490 [28], with an intermediate modulus of elasticity in comparison to the two previous adhesives. It should be noted that concerns about long-term performance or particular exposure conditions were not taken into account when these adhesives were selected. Based on their technical data sheets [26–28], Table 1 summarizes the most important characteristics of the adhesives used in this study, namely mechanical properties, viscosity, service temperature and application areas. All adhesives, later called by SikaForce, SikaDur and 3M for the sake of simplicity, were characterized according to EN ISO 527-2:2012 [29]. Therefore, five dumbbell shape specimens of each adhesive were casted and tested in tension at a constant speed of 1.0 mm/min until failure. A clip gauge (the same used for the characterization of the CFRP laminate) with stroke of 50 mm was placed at the central region of each specimen to measure its longitudinal deformation and, thereafter, to calculate the modulus of elasticity from the slope of the secant line between strain values of 0.05 % and 0.25 % of the stress-strain curve, according to EN ISO 527-1:2012 [30].

This study is included in a wider research project aiming at developing CFRP-annealed glass composite beams. Tempered glass was not considered suitable for this research, since the increase in tensile strength is associated with a severe decrease in the residual strength after crack initiation, which is undesirable for structural applications. Although heat-strengthened glass provides an interesting compromise between a relatively high tensile strength and a sufficiently large fragmentation pattern, this study is exclusively directed to the study of annealed glass applications. The annealed glass has been showing important economical (e.g. cheaper) and technical (e.g. it can be drilled or cut to accommodate unexpected changes in geometry) benefits to glass industry, particularly considering structural applications. On the other hand, laminated glass was also not considered since the study was focussed on the interaction between CFRP reinforcement and the glass substrate. Taking into account that the direct tension tests performed induce essentially pure tensile stresses in the glass sheets, the mechanical characterization of glass according to ISO 1288-3:2016 [31] was also not considered since it is based on bending tests which induce flexural stresses in the glass sheets.

2.2. Double-lap joint testing

The double-lap joint test configuration was adopted for the study of the bonded connections, since it minimizes the peel and cleavage stresses induced by shear stresses observed in the single-lap joint test configuration [17,32]. Therefore, this type of specimen geometry is beneficial for both brittle substrates (e.g. glass) and polymeric materials reinforced with unidirectional fibres (e.g. CFRP). Moreover, all glass sheets used in the double-lap joints were subjected to a grinding treatment of the edges, in order to eliminate flaws and defects derived from the cutting process and to avoid any accidents during their handling.

Fig. 1 shows the double-lap joint test configuration adopted. The specimens comprised two outer glass sheets 450 × 50 × 12 [mm] (length × width × thickness) and two inner CFRP laminates 450 × 50 × 1.2 [mm] (length × width × thickness), which were bonded together using the different adhesives under investigation (see Section 2.1). The bond test region was located at the connection between the glass sheet and the laminate of smaller length, designated as CFRP_I in Fig. 1. In order to avoid directly clamping the glass sheets to the gripping system of the testing machine, a bond rigid connection between the glass sheet and the laminate of larger length, CFRP_II, was used. In this rigid bond connection a considerably larger bond length between the CFRP and the glass was adopted (200 mm, at least four times higher than the maximum bond length studied), while in the bond test region the different bond lengths were studied. Furthermore, the two epoxy adhesives mentioned in Section 2.1 were used in the rigid bond connection to bond the components.

Regardless of the test configurations adopted, overlap lengths (bond length) of 15 mm (e.g. [33]), 25 mm (e.g. [19]) and 100 mm (e.g. [1,2]) were used in previous researches. Considering that the overlap length should be large enough to (i) be representative of the system and (ii) to neglect unavoidable defects, bond lengths of 25 mm and 50 mm were studied for all adhesives. The unavoidable defects previously mentioned may be related to porosity and voids in the adhesive, laminate end shape and spew fillet geometry [34], which increase the scatter of the measured properties if the bond length is reduced. In agreement with the recommendations of the technical data sheets of the adhesives, an adhesive layer thickness (t_a) of 0.3 mm and 1.0 mm was adopted for the adhesives Sikaforce and SikaDur, respectively (see Fig. 1c). The technical data sheet of the adhesive 3M DP490 does not provide any information regarding the recommended adhesive layer thickness to be used. A thickness of 0.3 mm was adopted in this case, according to the suggestion provided by the supplier.

The preparation of the specimens involved several steps. First, the CFRP laminates and glass sheets were cut. Subsequently, the bonding surfaces were carefully cleaned and degreased with acetone before bonding. After that, the adhesives were prepared according to the technical specifications and, then, they were applied with the assistance of a spatula. Then, both adherends were carefully assembled taking into account the alignment between them. In order to guarantee the correct bonding conditions during the application of the adhesive and the reinforcement, a constant pressure of 240 g/cm^2 was applied as a minimum bonding pressure [26]. Finally, the adhesives were subjected to post-cure conditions that comprised three stages: (i) 12-hour heating cycle, between

20 ºC and 50 ºC; (ii) 24-hour plateau at a constant temperature of 50 ºC; and (iii) 12-hour cooling cycle, between 50 ºC and 20 ºC. The post-curing protocol was aimed at (i) avoiding possible problems of testing specimens at slightly different ambient temperatures on the response of the CFRP-to-glass adhesively bonded joints; (ii) achieving further cure of the adhesives and, therefore, higher mechanical properties; and, (iii) minimizing the effect of testing specimens at different days. Furthermore, post-curing reproduces the long-term curing process that adhesives normally experience during their lifetime.

A total of 24 double-lap joints were prepared to be tested, with the following nomenclature: (i) SF-L25-i and SF-L50-i, for the i-th specimen with SikaForce adhesive and bond lengths of 25 mm and 50 mm, respectively; (ii) SD-L25-i and SD-L50-i, for the i-th specimen with SikaDur adhesive and bond lengths of 25 mm and 50 mm, respectively; and (iii) 3M-L25-i and 3M-L50-i, for the i-th specimen with 3M DP490 adhesive and bond lengths of 25 mm and 50 mm, respectively.

All tests were conducted in laboratory environment conditions at an average temperature and relative humidity of 18 ºC and 60 %, respectively. All test specimens were loaded in tension, under displacement control at a constant displacement rate of 1.0 mm/min (displacement between grips) until failure. All specimens were tested between 21 and 28 days after their production. The relative displacements between the laminate CFRP_I and the two glass sheets (slips) were measured using displacement transducers – Linear Variable Differential Transformer (LVDT) – with a stroke of 8 mm (linearity of 0.15 %), placed on the outer faces of both glass sheets, approximately 20 mm below the loaded end section (see Fig. 2). A Microtest PB2-F/200 kN load cell with precision of 0.01 kN was used to measure the load. Strain gauges (type: BFLA-5-3-3L by TML; gauge length: 5 mm; gauge factor: 2.08 ± 1 %) were installed on one specimen per series, on the outer faces of the glass sheets, at mid-length between the studied and rigid bond regions (see Fig. 2). The use of these sensors has two-fold objective: (i) verifying possible non-symmetric load distribution between the two glass sheets and (ii) determining the modulus of elasticity of the annealed glass (E_g), by inverse analysis.

In some of the specimens, Digital Image Correlation (DIC) technique was also used to document the evolution of the resistant mechanisms of the CFRP-glass hybrid systems, as well as to complement the understanding of the structural behaviour obtained from the double-lap joint tests. For this, a thin coating of white matt paint was applied over the region of interest, followed by the application of distributed black dots using spray paint. Only the adhesive connection was included in the region of interest. A Canon EOS 450D camera coupled with a Canon Zoom-EF 28-80mm *f*/3.5-5.6 IS lens was used to capture the images. A working distance (distance between the external face of the camera and the target surface) of 250 mm was adopted. Data was analysed with Correlate 2019 software [23]. For this purpose, the region of interest (ROI) shown in Fig. 3 was defined to perform the DIC analysis. The applied load and the relative displacements were measured at an average frequency of 100 Hz. Due to limitations on the acquisition system, the longitudinal strains in glass were measured at average frequency of 3 Hz. On the other hand, the images of the ROI were captured every 5 seconds during testing.

3. EXPERIMENTAL RESULTS

In this section, the experimental results derived from the mechanical characterization of the involved materials and from the double-lap joint tests are presented, analysed and discussed. Regarding the double-lap joint tests, in addition to the individual analysis of each series, the main advantages and disadvantages of each adhesive used are also discussed.

3.1. Glass, CFRP and adhesives

Table 2 shows the values of the mechanical properties obtained per material, namely the annealed glass, the CFRP laminate and the adhesives.

As previously described, the modulus of elasticity of the annealed glass was derived from the experimental results of double-lap joint tests through inverse analysis, and not directly obtained through experimental testing for example adopting the procedure suggested by ISO 1288-3:2016 [23]. Initially the tensile stress in glass (σ_g) was calculated assuming that the force imposed by the testing machine was equally distributed by both glass sheets ($F/2$). Then, the relationship $\sigma_g - \varepsilon_g$ was defined using the strain gauge measurements at the glass sheets. Finally, the modulus of elasticity of the annealed glass was calculated from the slope of the experimental response $\sigma_g - \varepsilon_g$ for glass sheets between strain values of 0.05 ‰ and 0.15 ‰. A Young's modulus (E_g) of 74 GPa was determined, which is consistent with the literature [35].

Regarding the CFRP laminates, all specimens tested showed linear elastic behaviour until failure, as expected. From these tests, a modulus of elasticity of 165.2 GPa and a tensile strength of 2418 MPa were obtained (see Table 2).

Regarding the adhesives, Sikaforce exhibited a significant nonlinear behaviour showing a clear tensile force plateau before the failure and, therefore, also a high deformation capacity (see Fig. 4a). On the other hand, SikaDur presented an essentially linear elastic behaviour until failure (see Fig. 4b), as well as stiffness and strength much greater than the ones previously shown by the polyurethane adhesive SikaForce (about 100 and 5 times, respectively). Finally, the 3M adhesive showed an intermediate behaviour between the two previously mentioned adhesives, with high tensile strength, similar to the SikaDur adhesive, and progressive loss of stiffness, resembling SikaForce, which guaranteed greater deformation capacity in comparison with SikaDur. The Poisson's ratios have not been experimentally determined in the present study. However, the values of 0.44, 0.30 and 0.38 are referred by Rodrigues [36], Haghani and Al-Emrani [37] and Nhamoinesu and Overend [19] for the Sikaforce, SikaDur and 3M, respectively. These values were adopted in the present study.

3.2. Double-lap joints

Fig. 5 shows the load (F) – loaded end slip (s_{le}) curves obtained from each series of double-lap joint tests. The bond responses obtained for each series differ significantly, as a result of the distinct behaviours of the different adhesives used and the bond lengths (L_b) adopted. On the other hand, Table 3 summarizes the results in terms of initial stiffness (K), maximum load (F_{max}) and corresponding displacement (d_{max}), as well as the observed failure modes. The initial stiffness of 3M and SD specimens were not significantly influenced by L_b. On the other hand, the 3M and SD series presented similar values of K, which were significantly higher than the values obtained from the SF series. The $F – s_{le}$ curves and the strain gauge measurements are compared in Fig. 6. As mentioned in Section 2.2, only one specimen per series was monitored using strain gauges. The two strain gauges of the SF-L25-I specimens captured an unexpected decrease in ε_{exp} without any decrease in F being recorded (see Fig. 6a). Regarding the other specimens, the tensile load (F) *vs*. longitudinal strain (ε_{exp}) relationship was linear until failure. Geometrical differences between the glass sheets (e.g. width) created small differences between the values measured by the two strain gauges of the same specimen.

Fig. 7 also shows the typical failure modes of each series observed during the present experimental programme. Four types of failure modes were clearly identified, which are related to the mechanical behaviour of the adhesive and the bond length, as well as the strength of the glass sheets. Table 3 also provides information about the failure modes of the experiments using the following nomenclature: I-AG, for adhesive failure by debonding at the interface adhesive/glass (see Fig. 8a); FT-L, for fibre-tear failure in CFRP laminate (see Fig. 8b); CS-G, for cohesive shear debonding in glass (see Fig. 8b); and C-G, for cohesive failure in glass.

As mentioned previously in Section 2, representative specimens of SD and SF series were monitored by documenting the surface of the specimens using digital images during the tests. Then, DIC method was used to extract the deformation fields at the surface of the specimens, in order to document unexpected phenomena and compare the differences in the behaviour of CFRP-glass composite systems when stiff and flexible adhesives are used. For the sake of simplicity, this paper presents only the results of one specimen per series. Furthermore, in order to perform more in-depth analyses, only specimens monitored with strain gauges were selected. In this sense, the specimens SF-L25-I and SF-L50-I (from flexible adhesive series) and SD-L25-I and SD-L50-I (from stiff adhesive series) were considered for the DIC analysis.

First, in order to verify the effectiveness of the DIC method in the scope of the present study, $F - s_{le}$ curves were extracted from the DIC analysis for one specimen per series and, subsequently, compared with the respective experimental curves (see Fig. 9). In line with the experimental monitoring setup shown in Fig. 2, s_{le} was determined measuring the displacement of the CFRP laminate at the loaded end section and the displacement of the glass sheets at 20 mm below this section, as close as possible to the outer faces. Similar $F - s_{le}$ curves were obtained from the DIC and LVDTs measurements (see Fig. 9). Considering s_{le} corresponding to F_{max}, relative differences between 1.6 % (SF-L50-I) and 18.8 % (SF-L25-I) were observed when comparing the DIC and LVDTs measurements. Minor deviations related to software calibration and image capture are the most likely reasons for the discrepancy observed between the two measurement strategies, as well as deformations induced by the loading procedure in the supports of the LVDTs, which are very small but noticeable at this scale. In addition, three-dimensional effects certainly contributed to the difference between DIC and LVDTs measurements.

Finally, relative slip curves, *s(x)*, along the bond length (L_b) were extracted from the DIC results, in order to identify differences between the bond behaviour of CFRP-glass systems when flexible and stiff adhesives are used (see Figs. 10 and 11). For the sake of simplicity, the *s(x)* curves were extracted only using the last image captured before failure.

3.3. Discussion of results

3.3.1. *Structural behaviour*

Both series SF-L25 and SF-L50 showed an almost linear behaviour at early stages of the bond response (see Fig. 5a and b), as a result of the chemical bond between the involved adherends (glass and CFRP). By increasing the bond length (from 25 to 50 mm) the initial stiffness increased ~50 %. All the SF-L25 specimens failed by adhesive failure at the interface adhesive/glass, while SF-L50 specimens collapsed by cohesive failure in glass. A noticeable loss of stiffness was observed before the SF-L25 specimens reached their ultimate load. Two reasons can explain this: (i) first, the expectable degradation of the chemical bond at increasing loads in all interfaces, mainly at the glass/adhesive interface; and, (ii) secondly, the nonlinear behaviour of the SikaForce adhesive (see Fig. 4a). In the case of SF-L50 series, the non-linear behaviour near the peak load was less pronounced since the failure was controlled by the glass rupture.

Regarding the SD-L25 and SD-L50 series (see Fig. 5c and d), in general, all specimens presented linear elastic behaviour until the failure, in line with the mechanical behaviour of the SikaDur adhesive (see Fig. 4b). Due to its high strength (5.3 times higher than in SikaForce), the progressive damage propagation from the loaded end to the free end was not significant. Nevertheless, regardless of the bond length, small plateaus were observed in the $F-s_{le}$ responses of some specimens. However, their bond stiffness remained essentially unchanged, excluding SD-L50-I. In these series, more complex failure modes were observed, always involving glass rupture (see also next section). SD-L50-I presented greater initial stiffness than other SD-L50 specimens (see Table 3). Fig. 12 shows the maximum principal strains at different stages of SD-L50-I $F-s_{le}$ response. The initiation of diagonal cracks is clearly identified. These cracks appeared at the vicinity of the loaded end section and progressively propagated towards the free end section during loading, creating short plateaus on the $F-s_{le}$ response of the SD-L50-I specimen. As referred previously, in contrast to other specimens, the bond stiffness of SD-L50-I decreased after the appearance of the first cracks (see Fig. 12c), resembling values displayed by the remaining SD-L50 specimens. By comparing SD-L50-I with SD-L50-II and SD-L50-III, higher initial stiffness is observed in the former. This can be explained by possible defects of the specimen (incorrect bond length and eventual misalignment of adherends). Apparently, the premature cracking pattern of glass sheets in the SD-L50-I specimen doesn't suggest the influence of geometric defects. Thereby, these unexpected cracks seem to have resulted from the combination of two aspects: (i) first, the high stiffness and strength of the SikDur adhesive, which prevented the progressive damage propagation from the loaded end to the free end and, in turn, the gradual transfer of tensile stresses from the CFRP laminate to the glass sheets, unlike the specimens with SikaForce; and, (ii) the lower strength of the glass close to the loaded end section, caused by the manufacturing process and handling of the glass pieces.

Regarding the 3M-L25 series (see Fig. 5e), all specimens presented a slight nonlinear behaviour prior to failure, in line with the mechanical behaviour of the 3M adhesive (see Fig. 4c). By increasing the bond length (from 25 to 50 mm) this slight nonlinear behaviour was not visible in 3M-L50 specimens (see Fig. 5f), since similar maximum loads were achieved in both series because the failure was controlled by the glass rupture. Due to the high strength of the 3M adhesive (similar to SikaDur), the progressive damage propagation from the loaded end to the free end and its impact in the shear response were not significant.

Comparing the 3M and SD series, both epoxy adhesives (SikaDur and 3M DP490) yielded similar initial stiffness (see Table 3), despite the more flexible response of the 3M adhesive when compared to the SikaDur (about 2.5 times – see Table 2). The difference between adhesive layer thicknesses adopted for each epoxy, which was about 3 times higher in SD series (1.0 mm) than in 3M series (0.3 mm), may explain this result. In contrast to the SD-L25 series, a slight loss of stiffness was observed in specimens of the 3M-L25 series, in line with the mechanical behaviour of the respective adhesive (see Fig. 4c). Due to the high strength of the 3M adhesive, the glass sheets failed before the theoretical peak-load of the adhesive connection was reached and, consequently, the possible post-peak curve of the response was not captured.

Regarding the maximum load, the values obtained from the SF-L25 specimens were significantly influenced by the adhesive behaviour and the bond length, since the CFRP-to-glass connection failed by debonding at the adhesive/glass interface (adhesive failure). The SF-L25 specimens showed the lowest average maximum load (17 kN) because they were produced using the adhesive with the lowest shear strength, as well as the shortest bond length among all tested bond lengths. In all other series, the specimens failed by cohesive failure in glass and/or fibre-tear failure in CFRP laminate and/or cohesive shear debonding in glass (see Fig. 7). Therefore, the average maximum loads reached in the specimen series produced with epoxy adhesives were mainly influenced by the mechanical properties of glass and CFRP.

Glass rupture was observed in all the specimens where 3M and SikaDur adhesives were used. However, substantial differences between the 3M and SD series were observed (see Table 3). In 3M series, the average maximum load increased from 28.4 kN to 31.7 kN (+11.6 %) when L_b was increased from 25 mm to 50 mm. In contrast, the maximum load remained almost unchanged in the case of SD series (SD-L25 *versus* SD-L50). On the other hand, considering similar bond lengths, both 3M series exhibited values of F_{max} significantly higher than the respective SD series, approximately 30% and 40% for bond lengths of 25 mm and 50 mm, respectively. The differences found are explained by the higher stiffness of the SikaDur adhesive, despite the natural scatter of the tensile strength of glass.

DIC analysis revealed that the bond test region of SD specimens that exhibited cracks close to the loaded end was completely shattered. Due to the brittle nature of the annealed glass, the formation of these cracks occurred very suddenly, releasing large amounts of energy and, in turn, increasing the dynamic response of the specimens. For high loading levels (>20 kN), the glass was unable to accommodate the energy released by the crack propagation from the loaded end to the free end and, consequently, the glass sheets failed in an uncontrolled manner, shattering the entire bond test region (see Fig. 7). Due to the brittle nature of the annealed glass which shows no softening, similar maximum loads were achieved in both SD series, where the failure was governed by the loading level at the instant corresponding to the initiation of new cracks near the loaded end. Although a smoothing of the stress concentration near the loaded end section was expected with increasing bond length, the SD-L50 series presented a slightly lower maximum load in comparison with the SD-L25 series, probably due to the high scatter of the tensile strength of glass.

Comparing the $F - s_{le}$ curves of SD-L25 and 3M-L25 series with the corresponding responses of SF-L25 series, significantly higher values of the initial stiffness and maximum load were obtained with the stiff adhesives, while significantly higher values of s_{le} corresponding to F_{max} were achieved with the polyurethane adhesive. The results also show that the increase in L_b from 25 to 50 mm resulted in higher values of K of the CFRP-to-glass connections. The SF-L50, SD-L50 and 3M-L50 series showed initial stiffness values 48.6 %, 19.3 % and 13.9 % higher than the counterpart series with L_b of 25 mm, respectively.

3.3.2. *Failure modes*

Regardless of the bond length, 3M adhesive specimens always failed by cohesive failure in glass (see Table 3). In the case of SF specimens, all SF-L50 specimens failed by cohesive failure in glass as well, while SF-L25 specimens always failed due to debonding at the adhesive/glass interface (see Fig. 8a) after facing an extensive loaded end slip. Regarding the SD specimens, cohesive shear debonding in glass and fibre-tear failure in CFRP (see Fig. 8b) was observed in all specimens excluding SD-L25-III and SD-L25-IV, where the glass failed due to cohesive failure.

While the glass sheets of the SF-L50 specimens failed outside the bond test region (tensile failure), the SF-L25 specimens always failed by debonding at the adhesive/glass interface (see Fig. 8a). In all SF-L25 specimens one glass sheet failed immediately after the peak-load was achieved. Therefore, SF-L25 specimens did not show post-peak response (softening). As discussed subsequently, this can be explained by two distinct effects: (i) the asymmetric behaviour of the bond test region and (ii) the eccentric loading at the glass sheets.

The asymmetric behaviour of the bond test region was observed in all specimens. However, due to the low stiffness of SikaForce and progressive damage at the adhesive/glass interface, it was more evident in structural responses of SF-L25 specimens. The loss of symmetry in double-lap joints can be explained by several factors, namely: (i) deviations in the width of glass sheets related to their manufacturing process; (ii) variations in the edges' treatment of the glass elements, causing small differences between the bonding surfaces; and, (iii) finally, the adhesive thickness adopted in SF specimens was very thin (0.3 mm), and small differences between the thicknesses of both adhesive joints may have caused a considerable difference between their stiffnesses.

As shown in Fig. 6a, the loss of stiffness in SF-L25-I (F > 5.0 kN) seems to have resulted in a decrease in the longitudinal strain of the glass (ε_{exp}) captured by the strain gauge measurements. It should be noted that this effect only occurred in specimens with flexible adhesive (low stiffness) and L_b equal to 25 mm. Therefore, the lower the adhesive stiffness and the bond length, the higher the non-linearity observed in the $F - \varepsilon_{exp}$ responses. On the other hand, when SF-L25-I started to show stiffness decay, the slip at the loaded end measured by LVDTs was consistently greater than the values captured by DIC (see Fig. 9a). This effect may be explained by an increasing rotation of the LVDTs supports relatively to the loading axis (see Fig. 13a).

Taking into account the double-lap joint geometry (see Fig. 1), the load was transferred from the CFRP laminate to the glass sheets through shear stresses in the adhesive joints, inducing an eccentric loading in the glass sheets with eccentricity (e) approximately equal to 6.9 mm. The eccentricity effect yielded tensile stresses at the inner faces and compression stresses at the outer faces (lateral bending). In this sense, relative horizontal displacement curves between the two glass sheets and the CFRP laminate were extracted using the DIC method (see Fig. 13). For the sake of simplicity, only the last image captured before the SF-L25-I failure was considered. According to Fig. 13, when SF-L25-I achieved F_{max}, the average horizontal displacement at the loaded end section was 18 % of s_{le}. For each glass sheet, the incremental strain (ε_{incr}) caused by the eccentricity effect was calculated according to the double integration method from the relative horizontal displacement curves shown in Fig. 13. On the other hand, the longitudinal strain (ε_{lin}) that would be expected without flexural stresses was calculated assuming E_g equal to 74 GPa and considering the symmetrical behaviour of the bond test region. According to Table 4, the difference between ε_{exp} and ε_{lin} was entirely caused by the eccentricity effect. As the asymmetric behaviour of the bond test region is common to all specimens, regardless of the adhesive, it is reasonable to assume that the significant lateral bending of the glass sheets in SF-L25-I resulted from the flexible behaviour of the SikaForce adhesive and its low strength. The lateral bending of the glass sheets induced cleavage stresses in the adhesive joints, increasing the progressive damage from the loaded end to the free end. The higher the adhesive damage, the higher the flexural stresses in the glass sheets and, in turn, the cleavage stresses in the adhesive joints.

In the case of the 3M and SD series, although similar values of initial stiffness were observed in both cases, the two epoxy adhesives showed distinct failure modes. While the 3M specimens failed due to the glass rupture below the bond region (tensile failure), the SD specimens failed by cohesive shear debonding in substrates. Excluding SD-L25-II and SD-L25-IV, which failed by cohesive failure in glass, the bond region of the specimens with SikaDur was completely shattered (see Fig. 7). As inferred in Section 3.3.1, this resulted from the higher stiffness of the SD adhesive (when compared to 3M). Regardless of the bond length, the failure of SD specimens was mainly induced by dynamic effects resulting from the initial cracking of the glass sheets near the loaded end section.

3.3.3. *Stiff vs. flexible adhesives*

Figs. 10 and 11 compare the slip profiles along the bond length between SF and SD series extracted from the DIC analysis. When SD adhesive is used for glass-to-CFRP connections, the damage progression affects also the surrounding glass (cracking from the loaded end to the free end). On the other hand, the application of SF results in concentration of damage mainly at the adhesive. A significant slip at the free end section (s_{fe}) was observed in both specimens with SF, the most flexible adhesive. This is the result of a more uniform distribution of bond stresses along L_b when flexible adhesives are applied, due to the lower stiffness of the material. In contrast, the values of s_{fe} in SD specimens were substantially lower when compared to s_{le}. This is likely the result of the high stiffness of stiff adhesives, which led to high bond stresses near the loaded end section and very low bond stresses near the free end section, creating a non-uniform distribution of bond stresses along L_b. Due to the significantly higher stiffness of the CFRP laminate when compared to the polyurethane adhesive, the transmission of the tensile force from the CFRP to the glass sheets occurs in a smoother way. In contrast, the high stiffness of SikaDur adhesive leads to a greater stress concentration at the glass sheets, which may have led to the initiation of cracking in glass even before the L_b was entirely mobilized.

4. ANALYTICAL MODELLING

This section is dedicated to the study carried out to analytically estimate the local bond stress-slip ($\tau - s$) law and the maximum load (F_{max}) *vs*. bond length (L_b) response for each adhesive type, considering the experimental results obtained from the double-lap joint tests.

4.1. Description of the method

Despite the three-dimensional character of CFRP-to-glass adhesive bond, in order to decrease the level of complexity of the theoretical formulations [38], 1D strategy is usually adopted to analytically model the bond behaviour. According to e.g. Focacci *et al*. [39], Russo *et al*. [40] and Sena-Cruz and Barros [41], the local bond phenomenon between the CFRP laminate and the glass can be characterized mathematically by a second order differential equation in terms of slip (see Eq. (1)). According to Sena-Cruz [38] and Sena-Cruz and Barros [41], Eq. (1) was derived assuming that CFRP laminate behaves linearity in its longitudinal direction and neglecting the substrate (in this case glass) and adhesive deformability. Despite the flexibility of SikaForce when compared to epoxy adhesives, for the sake of simplicity, the deformability of the adherends was neglected.

$$\frac{d^2s}{dx^2}=\frac{P_f}{E_f A_f}\tau(x) \tag{1}$$

A computational application previously developed by Sena-Cruz and Barros [41] was used to define the $\tau - s$ relationships for the three adhesives. Using an inverse analysis strategy complemented with numerical fitting tools, this computational application performs several iterations until it finds the parameters required by the $\tau - s$ relationship that satisfy Eq. (1), where $\tau(x) = \tau(s(x))$ is the shear stress between the CFRP laminate and adhesive as a function of the relative slip along the bond length. Moreover, E_f and A_f are the Young's modulus and the cross-section area of the reinforcement element, respectively, and P_f is the perimeter of the reinforcement in contact with adhesive.

A brief description about the iterative procedure used by the computational application to determine the best parameters that define the $\tau - s$ relationship is given, as follows: (i) first, based on the experimental responses, the user sets a range of values for each required parameter by the $\tau - s$ relationship adopted; (ii) then, the computed $F - s$ response is determined for the free and loaded ends; (iii) later, the difference between the computed and experimental responses is calculated in terms of the peak load and the corresponding slip and the area difference between both curves (experimental and computed); and (iv) finally, this process is repeated until an acceptable accuracy is obtained, according to a pre-defined residual criteria defined by the user. More details about this algorithm may be found in Sena-Cruz [38] and Cunha *et al*. [42].

A CFRP-to-glass bonded joint is shown in Fig. 14, where L_b is the bond length, F is the load and s_{fe} and s_{le} are the slips at the free and loaded end sections, respectively. By using this tool, the following involved parameters can be access along the bond length: the slip, $s(x)$; the shear stress at the interface, $\tau\,(x)$; the axial strain in CFRP, $\varepsilon_f\,(x)$; and the axial force at the CFRP, $F(x)$. Finally, F is calculated using Eq. (2), which was obtained by equating the internal work due to the elastic deformation of the CFRP and the external work produced by the shear stress profile created at the interface [42].

$$F=\sqrt{\left(2.E_f.A_f.P_f.\int_{s_f}^{s(s=L_b)}\tau(s)ds\right)} \tag{2}$$

4.2. Local bond stress-slip relationship

Several authors (e.g. [43–46]) have evaluated the efficiency of different $\tau - s$ laws in the simulation of the local behaviour for FRP-to-concrete interfaces. Given the lack of specific $\tau - s$ relationships to simulate the debonding of CFRP-to-glass interfaces, several bond stress-slip laws that exist in the literature were considered in this study. The local $\tau - s$ laws were selected considering the following criteria: (i) the behaviour of adhesive; (ii) the type of response of the double-lap joints before the peak load is reached; (iii) the typically smooth surfaces of both adherends, suggesting the absence of friction stresses at the CFRP/adhesive or glass/adhesive interfaces; and (iv) the amount of interfacial fracture energy, which should be as low as possible for conservative reasons, taking into account the last two criteria.

As the stiffness of double-lap joints with SikaDur remained unchanged until they failed, their adhesive interfaces were modelled analytically considering a linear $\tau - s$ relationship, defining only the shear stiffness (K_τ). On the other hand, considering the abovementioned criteria, for the SikaForce and 3M adhesives, which showed nonlinear behaviour in direct tension tests (see Fig. 4c) and in double-lap joints (see Fig. 5e), the $\tau - s$ exponential law proposed by Dimande [47] (see Eq. (3)) was used to solve Eq. (1). According to Eq. (3), two parameters are required to define the $\tau - s$ relationship proposed by Dimande [47]: the bond strength, τ_m, and its corresponding slip, s_m. These parameters were calibrated for the average experimental curve of each series with the L_b of 25 mm. Regarding the CFRP laminate, values of 92 mm (46 mm with each glass sheet) and 60 mm^2 for P_f and A_f were adopted, respectively.

$$\tau(s)=\tau_m \cdot \frac{s}{s_m} . e^{1-\frac{s}{s_m}} \tag{3}$$

In 3M series, the glass sheets ruptured before the failure of the CFRP-to-glass interfaces was reached. Consequently, the $\tau - s$ relationship proposed by Dimande [47] could not be determined for the 3M adhesive, since an infinite number of $\tau_m - s_m$ combinations could be calibrated for each $F - s_{le}$ curve. To overcome this, the finite element software ABAQUS/Explicit [24] was used to determine τ_m. For this purpose, the 3M adhesive was simulated as an isotropic elastic material. Its nonlinear behaviour (see Fig. 4c) was taken into account using a VUSDFLD subroutine, developed to redefine the Young's modulus at each material point as a function of its maximum principal strain. Other assumptions adopted in these numerical simulations can be found later in Section 5. Fig. 15 shows the diagram of shear stresses along L_b when the maximum principal stress at the loaded end section reaches the tensile strength of the 3M adhesive (32.8 MPa). From Fig. 15, the value of 19.6 MPa was adopted for τ_m.

Table 5 presents the parameters that define the $\tau - s$ relationship for each adhesive, as well as the normalized error, Err, i.e. the ratio between the area limited by the experimental and computed responses. The experimental and computed $F - s_{le}$ responses are compared in Fig. 5, for both 25 mm and 50 mm bond lengths. The bond behaviour of CFRP-glass composite systems was well described by the analytical models adopted: (i) the Dimande’s $\tau - s$ relationship when flexible (e.g. SikaForce) and stiff (e.g. 3M) adhesives with nonlinear behaviour are used; and (ii) the linear $\tau - s$ relationship for stiff adhesives (e.g. SikaDur) with linear behaviour until failure and high strength. Fig. 5 also demonstrate that parameters found for the $\tau - s$ relationships are independent of the bond length (the laws were calibrated for L_b = 25 mm and used for L_b = 50 mm).

4.3. Effective bond length

In composite systems, the load is transferred to the reinforcement element by means shear stresses in the adhesive layer, mostly near the loaded end. When the applied load increases, the adhesive close to the loaded end is damaged and the active bond length shifts to a new zone, towards the free end, indicating that only part of the adhesive bond is effective.

Considering design purposes of CFRP-glass composite systems, the maximum load (F_{max}) as a function of the anchorage length of CFRP laminate was determined for the three adhesives. For this purpose, the computational programme abovementioned as well as the previously calibrated $\tau - s$ relationships were used. As presented in Fig. 16, F_{max} no longer increases when L_b is extended to values above the effective bond length (l_{eff}), which is approximately 400 mm and 150 mm for SikaForce and 3M adhesives, respectively. The $F_{max} - L_b$ curve was not depicted for CFRP-glass connections with SikaDur because their interfaces were analytically modelled using a linear $\tau - s$ relationship, neglecting any adhesive damage. Therefore, F_{max} is infinite for $L_b > 0$.

5. NUMERICAL ANALYSIS

5.1. Initial considerations

Numerical analysis were performed using the finite element method, in order to verify the effectiveness of the local bond-slip laws determined in Section 4 for the simulation of CFRP-glass composite structural elements and, in addition, to obtain the profile of shear stresses along the bond length. Therefore, cohesive elements were used to simulate the non-linear behaviour of the interfaces (CFRP/adhesive and adhesive/glass) and the adhesive itself. The results obtained from the numerical simulations provide additional information regarding the bond behaviour of CFRP-to-glass adhesively bonded joints. Moreover, the parameters determined from the analytical study (see Section 4) were recalibrated taking into account some aspects that influenced the experimental measurements in F - s_{le} curves. Similarly to the analytical approach presented in Section 4, the results of the numerical results were compared with the experimental ones.

All numerical simulations were performed in ABAQUS/Standard software [24], using material models available in the software's library. ABAQUS/Explicit was not considered due to its mesh limitations, since only finite elements with reduced integration could be used and therefore would affect the accuracy of the numerical models in this particular case.

5.2. FE model description

The double-lap joint tests were simulated with following assumptions: (i) two-dimensional (2D) problem, with different out-of-plane widths for the three elements, in order to consider the influence of the edges treatment on the adhesive layer's width; (ii) only one adhesive interface was considered, assuming symmetrical behaviour for both CFRP-to-glass interfaces with respect to the longitudinal axis of the specimen. Fig. 17 shows the geometry, boundary conditions and load configuration.

The annealed glass and CFRP were simulated as an isotropic materials with linear elastic constitutive laws, both in tension and in compression. A Young's modulus (E_g) of approximately 70 GPa and a Poisson's ratio (ν_g) of 0.23 should be used to describe the linear elastic behaviour of annealed glass, in accordance with the recommendations of the Guideline for European Structural Design of Glass Components [35]. Based on the results measured by the strain gauges from the double-lap joint tests, a Young's modulus (E_g) of 74 GPa was adopted (see Table 2). Regarding the CFRP, a Young's modulus, E_{CFRP}, of 165.2 GPa was adopted (see Table 2) and a Poisson's ratio, ν_{CFRP}, of 0.28 was assumed, according to its technical data sheet.

5.2.1. *Adhesive interface*

The CFRP-to-glass interfaces were modelled using "*cohesive elements*". Their constitutive response was defined using a "*traction-separation approach*". Although the traction-separation approach is more suitable to model delamination at bonded interfaces where the interface thickness is negligibly small, this option was used because the "*continuum approach*" only allows to simulate the material damage and failure in ABAQUS/Explicit [24], which was not considered at this stage.

The traction-separation approach assumes that failure of the cohesive elements is characterized by progressive degradation of the material stiffness driven by a damage process [24]. A linear elastic behaviour is initially considered by the abovementioned approach. An uncoupled behaviour between the normal and shear components was defined for these simulations. Therefore, the linear elastic normal stiffness (K_σ) and the linear elastic tangential stiffness (K_τ) were derived from the mechanical characterization (see Section 3.1) and double-lap joint tests (see Section 3.2), respectively. The adopted constitutive relationship to simulate CFRP-to-glass interfaces is governed by Eq. (4), where $\Delta\sigma_n$ and Δu_n are increments of stress and displacement in the normal direction to the interface, while $\Delta\tau_s$ and Δs_s are increments of stress and displacement in the tangential direction to the interface, respectively.

$$\begin{bmatrix}\Delta\sigma_n\\ \Delta\tau_s\end{bmatrix}=\begin{bmatrix}K_\sigma & 0\\ 0 & K_\tau\end{bmatrix}\begin{bmatrix}\Delta u_n\\ \Delta s_s\end{bmatrix} \tag{4}$$

According to ABAQUS [24], the failure mechanism is controlled by (i) the damaged initiation criteria and (ii) the damaged evolution law. For the former, a "*maximum nominal stress criterion*" was adopted, i.e. the damage initiates when the maximum nominal stress ratio reaches either the normal strength (σ_m) or the shear strength (τ_m), according to Eq. (5). For the latter, the damage factor was specified as a function of the displacement in relation to the effective displacement at damage initiation, using the $\tau - s$ relationships derived in Section 4.2.

$$max\left\{\frac{\sigma}{\sigma_m},\frac{\tau}{\tau_m}\right\}=1 \tag{5}$$

5.2.2. *Mesh strategy*

Both glass sheets and the CFRP laminate were simulated using 4-node plane stress elements with a 2 × 2 integration scheme (CPS4). 4-node two-dimensional cohesive elements with two integration points (COH2D4) were used to simulate the adhesive layer. As shown in Fig. 17, special attention was paid to the mesh in the overlap zone to ensure a sufficient refinement. Therefore, finite elements ranging in size from 0.25 (width) × 0.25 (height), near the adhesive interface, to 1.0 (width) × 1.0 (height) [mm] were used in these numerical simulations.

5.3. Numerical results

In the experimental tests, the LVDTs used to measure the slip at the loaded end were placed on the external faces of the glass sheets, about 20 mm below the free end section (see Fig. 2). Thereby, the experimental measurements of the slip at the loaded end section (see Fig. 5) included also the longitudinal deformation of glass sheets between the loaded end section and the LVDTs section (~20 mm), as well as the three-dimensional effects that had occurred (e.g. lateral deflection of glass sheets). In contrast, the numerical model allows to take the measurement of the slip directly at the loaded end section, without the physical constrains that the experimental model imposes. Thus, in order to simulate the behaviour of the double-lap joints, an iterative procedure was initially adopted to find a s_{eff} corresponding to τ_m, where s_{eff} is the effective slip that would be experimentally obtained if the LVDTs could be physically placed on the inner faces of the glass sheets at the loaded end section. The initial stiffness was the criteria used to find s_{eff}. The iterative procedure ended when the initial stiffness obtained from the $\tau - s_{eff}$ law *versus* LVDTs section (outer face) reached the initial stiffness obtained from the $\tau - s$ law *versus* loaded end section (inner face). The maximum relative difference between these two initial stiffnesses was limited to 1.0 %. All numerical results presented later were obtained taking into account the $\tau - s_{eff}$ relationships based on the parameters shown in Table 6.

For the sake of simplicity, only the iterative procedure applied to the SF-L25 series is covered in detail in this paper, showing its initial ($\tau - s$ law) and final ($\tau - s_{eff}$ law) stages in Fig. 18b and Fig. 18c, respectively. According to Fig. 18a, $d_{CFRP,le\text{-}s}$ and $d_{g,le\text{-}s}$ are, respectively, the longitudinal displacements of CFRP laminate and glass (inner face) at the free end section and $d_{g,LVDT\text{-}s}$ is the longitudinal displacement of glass at the LVDTs section (outer face). Called "Ref." in Fig. 18, the reference $F - s_{le}$ curve to find s_{eff} was initially defined by subtracting $d_{CFRP,le\text{-}s}$ to $d_{g,le\text{-}s}$, both obtained from the $\tau - s$ law. On the other hand, the object $F - s_{le}$ curve, called "Obj." in Fig. 18, was determined at each iteration by subtracting $d_{CFRP,le\text{-}s}$ to $d_{g,LVDT\text{-}s}$, both derived from the bond stress – slip law considered in this iteration. Fig. 18 shows that the longitudinal deformation of glass influenced significantly the experimental responses captured by LVDTs. However, due to the brittle nature of glass, it would be very difficult to implement another measurement strategy.

As shown in Fig. 19, the numerical models simulated with great accuracy the experimental behaviour of each series of double-lap joints when the $\tau - s_{eff}$ relationships were used. This shows that the analytical parameters shown in Table 6 are effective when used in numerical simulations. Further studies of CFRP-to-glass interfaces, as well as numerical simulations of CFRP-glass composite systems (e.g. beams) are possible using this approach.

Furthermore, the relative slips along L_b extracted using the DIC method, $s_{DIC}(x)$, and the ones obtained from the numerical simulations, $s_{NS}(x)$, were compared for the specimens SF-L25-I, SD-L25-I and 3M-L25-I. The $s_{DIC}(x)$ and $s_{NS}(x)$ curves were defined using the last image captured and the maximum load step, respectively. Since the parameters presented in Table 6 were obtained using the average $F - s_{le}$ curve of each series and individual specimens are expected to show a scatter in the overall response magnitudes, the dimensionless curves $s_{NS}(x) / s_{NS}(x = 0)$ and $s_{DIC}(x) / s_{DIC}(x = 0)$ were considered. This strategy was also followed for other properties. Thus, this analysis was mainly focussed on the shape of $s(x)$ and, consequently, on the distribution of longitudinal strains in the CFRP laminate, $\varepsilon_{CFRP}(x)$, and shear stresses in the adhesive layer, $\tau(x)$.

The axial strain distributions in the CFRP laminate along L_b were previously determined using the differential equation that characterizes the local bond phenomenon (see more details in Section 3.3). According to Sena-Cruz [38], considering the linear elastic behaviour of the reinforcement and neglecting the deformability of adhesive and glass, $\varepsilon_{CFRP,DIC}(x)$ can be obtained thought Eq. (6). $s_{DIC}(x)$ is shown in Fig. 10 for the SF-L25-I and SD-L25-I specimens.

$$\varepsilon_{CFRP,DIC}=\frac{ds_{DIC}(x)}{dx} \tag{6}$$

As shown in Fig. 20, the DIC technique and the numerical models were able to capture the bond behaviour between the adherends, providing similar distributions in terms of either slip or longitudinal deformations in the CFRP laminate along the bond length. As $\varepsilon_{CFRP}(x)$ is linear in SF-L25-I (see Fig. 20a), $\tau(x)$ is approximately constant along L_b due to its flexibility. However, in SD-L25-I, $\varepsilon_{CFRP}(x)$ is governed by a quadratic equation (see Fig. 20b) and, consequently, $\tau(x)$ is not constant along L_b. High shear stresses occurred close to the loaded end of the double-lap joints using SikaDur, about 2 times greater than the shear stresses at the free end. As discussed in Section 3.3, when stiff adhesives showing linear elastic behaviour are used, the performance of CFRP-glass composite systems is more susceptible to the local features of glass (e.g. tensile strength, edge treatment and density of micro-cracking). On the other hand, the 3M adhesive shows an intermediate type of response that is characterized by being not flexible enough for $\tau(x)$ in 3F-L25-I to be constant, like in the case of SF-L25-I, although flexible enough to avoid high shear stress concentrations near the loaded end, as in the case of SD-L25-I.

According to Machalická and Eliášová [17], the shear stresses pattern depends on (i) the geometry of the double-lap joints, that is, the overlap length and the adhesive thickness, (ii) the mechanical properties of the adhesive and (iii) the stiffness of adherend materials and their thicknesses. In order to evaluate the influence of the overlap length in each adhesive, the $\tau(x) / \tau(x = 0)$ curves were compared in Fig. 21 according to following criteria: (i) similar loads during pre-peak response were considered to extract the distribution patterns of both series of each adhesive; and (ii) the two $\tau(x)$ curves of each adhesive were normalized using $\tau(x = 0)$ corresponding to L_b of 25 mm.

According to Fig. 21, when the stiff adhesives are used, the shape of the shear stress distribution diagrams are significantly influenced by L_b, but the bond stress at the loaded end remains almost constant, since the tensile stress transfer length is smaller. On the other hand, with the polyurethane adhesive, $\tau(x)$ is mainly influenced by L_b in terms of value, since for the investigated overlap lengths the shear stresses remains almost constant along L_b due to the flexibility of the adhesive.

6. CONCLUSIONS

In this research work, the structural performance of CFRP-to-glass adhesively bonded joints using different adhesives was experimentally studied. For this purpose, double-lap joints with two bond lengths (25 and 50 mm) were produced and then tested in tension. Considering only structural adhesives that ensure high interaction between the glass and the CFRP, three adhesives were selected to comprise a wide range in terms of material stiffness: (i) the SikaForce L100 7100 (SF), flexible polyurethane adhesive; (ii) the SikaDur 330 (SD) stiff epoxy adhesive; (iii) the 3M DP490 (3M) stiff epoxy adhesive. In addition, analytical and numerical investigations were performed to determine the local bond stress-slip law for each adhesive type, and to extend the analysis of the experimental results. The main conclusions can be summarized as follows:

- Comparing the experimental responses obtained with stiff and flexible adhesives, significant differences were found in terms of initial stiffness, maximum load and corresponding slip for the studied bond lengths. Due to the linear elastic behaviour of the SikaDur adhesive, the SD double-lap joints showed linear behaviour until failure of the glass, while in the other series of specimens a progressive loss of stiffness for increasing load was observed. A noticeable higher slip at maximum load was achieved in joints with SikaForce, the most flexible adhesive. The high deformation capacity of this adhesive can contribute to increase the ductility of CFRP-glass composite systems (e.g. beams). For these materials and specimen configuration, it was not possible to obtain post-peak (softening) behaviour.
- While debonding at the glass/adhesive interface and cohesive failure in glass occurred in all SF-L25 and SF-L50 joints, respectively, all 3M specimens failed due to the glass cohesive failure in tension, between the rigid and studied bond regions. In the case of the SD series, a mixed failure mode combining cohesive shear debonding in glass and fibre-tear failure in CFRP was observed, due to the high concentration of shear stresses close to the loaded end caused by high stiffness of the SikaDur adhesive. The failure modes could be deducted from the obtained distributions of shear stresses along the bond length which, in turn, were also clearly influenced by the adhesive type, with uniform patterns for the flexible adhesive and non-uniform patterns for the epoxy adhesives, mainly in joints with SikaDur.
- When stiff adhesives with linear elastic behaviour are used in CFRP-to-glass adhesively joints, their bond behaviour is much more susceptible to the local mechanical properties and features of glass (e.g. tensile strength, edge treatment quality, density of micro-cracking and localized damage during handling). As the glass is a heterogeneous material in terms of its tensile strength, the adhesives must combine two

essential features to improve the structural performance of CFRP-to-glass connections: (i) high shear strength and (ii) considerable deformation capacity.

- Extremely stiff responses of the adhesives, e.g. SikaDur, can impair the ductile performance of CFRP-glass composite systems (e.g. beams) after cracking, since they are less effective in distributing the shear stresses throughout longer bond lengths and, therefore, do not promote stress redistribution mechanisms. However, this characteristic is also related to the type of reinforcement used.
- The adopted analytical model was capable of predicting the local bond-slip laws of CFRP-glass composite systems with good accuracy for all adhesives, using a linear $\tau - s$ relationship for stiff adhesives with linear behaviour until failure (e.g. SikaDur) and the Dimande's exponential $\tau - s$ relationship for flexible adhesives (e.g. SikaForce), as well as stiff adhesives with nonlinear behaviour (e.g. 3M).
- Regardless the tensile strength of the CFRP laminates and glass used, the maximum load *vs*. bond length curves were defined for specimens with 3M and SikaForce adhesives and the effective bond lengths of approximately 150 and 400 mm were found, respectively. This allowed to define the required anchorage length as a function of the ultimate limit state conditions.
- The numerical model for CFRP-to-glass interfaces showed very good predictive performance for all the simulated double-lap joints. Furthermore, it allowed to determine the effective loaded end slip, as well as to quantify the effects of the longitudinal deformation of the glass sheets and three-dimensional effects (e.g. lateral deflection of the glass sheets) experimentally measured. Therefore, it was possible to determine the effective local bond-slip law for each adhesive.
- The approach followed in this study, including the experimental characterization of the bond behaviour of the adhesives, the derivation of the analytical local bond laws, and the numerical simulation of the CFRP-to-glass interfaces, was found useful for the modelling of CFRP-glass composite systems with good accuracy. This may contribute to the structural design of larger scale reinforced glass composite systems.

ACKNOWLEDGEMENTS

The first author also wishes to acknowledge the grant SFRH/BD/122428/2016, provided by Fundação para a Ciência e a Tecnologia, IP (FCT), financed by European Social Fund and by national funds through the FCT/MCTES. Finally, the authors also like to thank the COVIPOR – Companhia Vidreira do Porto Lda., S&P Clever Reinforcement Iberica Lda. and SIKA for supplying the materials.

REFERENCES

[1] Correia J, Valarinho L, Branco F. Post-cracking strength and ductility of glass-GFRP composite beams. Compos Struct 2011;93:2299–309.

[2] Valarinho L, Correia J, Branco F. Experimental study on the flexural behaviour of multi-span transparent glass-GFRP composite beams. Constr Build Mater 2013;49:1041–53. https://doi.org/10.1016/j.conbuildmat.2012.11.024.

[3] Balan B, Achintha M. Experimental and Numerical Investigation of Float Glass-GFRP Hybrid Beams. In: Belis, Bos, Louter, editors. Challeging Glas. 5 - Conf. Archit. Struct. Appl. Glas., vol. 97, Ghent: 2016, p. 281–96. https://doi.org/10.2514/6.2009-5462.

[4] Biolzi L, Orlando M, Piscitelli LR, Spinelli P. Static and dynamic response of progressively damaged ionoplast laminated glass beams. Compos Struct 2016;157:337–47. https://doi.org/10.1016/j.compstruct.2016.09.004.

[5] Cruz P, Pequeno J. Structural Timber-Glass Adhesive Bonding. Challenging Glas., 2008, p. 205–14.

[6] Cruz P, Pequeno J. Timber-Glass Composite Beams: Mechanical Behaviour & Architectural Solutions. Challenging Glas., 2008, p. 439–48.

[7] Belis J, Callewaert D, Delincé D, Impe R Van. Experimental failure investigation of a hybrid glass / steel beam. Eng Fail Anal 2009;16:1163–73. https://doi.org/10.1016/j.engfailanal.2008.07.011.

[8] Bos F, Veer F, Hobbelman G, Louter P. Stainless steel reinforced and post-tensioned glass beams. ICEM12- 12th Int. Conf. Exp. Mech., Bari, Italy: 2004, p. 1–9.

[9] Louter C, Belis J, Veer F, Lebet J. Structural response of SG-laminated reinforced glass beams; experimental investigations on the effects of glass type, reinforcement percentage and beam size. Eng Struct 2012;36:292–301. https://doi.org/10.1016/j.engstruct.2011.12.016.

[10] Louter C, Cupac J, Lebet J. Exploratory experimental investigations on post-tensioned structural glass beams. J Facade Des Eng 2014;2:3–18. https://doi.org/10.3233/FDE-130012.

[11] Louter C, Cupac J, Debonnaire M. Structural glass beams prestressed by externally bonded tendons. Glas. Glob. Conf. Proc., Philadelphia, EUA: GlassCon Global; 2014, p. 450–9.

[12] Palumbo M. A New Roof for the XIIIth Century 'Loggia de Vicari' (Arquà Petrarca – PD Italy) Based on Structural Glass Trusses: A Case Study. Glas. Process. Days, Tempere, Finland: 2005.

[13] Neto P, Alfaiate J, Valarinho L, Correia J, Branco F, Vinagre J. Glass beams reinforced with GFRP laminates: Experimental tests and numerical modelling using a discrete strong discontinuity approach. Eng Struct 2015;99:253–63. https://doi.org/10.1016/j.engstruct.2015.04.002.

[14] Valarinho L, Sena-Cruz J, Correia J, Branco F. Numerical simulation of the flexural behaviour of composite glass-GFRP beams using smeared crack models. Compos Part B Eng 2017;110:336–50. https://doi.org/10.1016/j.compositesb.2016.10.035.

[15] Achintha M, Balan B. Characterisation of the mechanical behaviour of annealed glass – GFRP hybrid beams. Constr Build Mater 2017;147:174–84. https://doi.org/10.1016/j.conbuildmat.2017.04.086.

[16] Keller T, De Castro J. System ductility and redundancy of FRP beam structures with ductile adhesive joints. Compos Part B Eng 2005;36:586–96. https://doi.org/10.1016/j.compositesb.2005.05.001.

[17] Machalická K, Eliášová M. Adhesive joints in glass structures: effects of various materials in the connection, thickness of the adhesive layer, and ageing. Int J Adhes Adhes 2017;72:10–22. https://doi.org/10.1016/j.ijadhadh.2016.09.007.

[18] Louter C, Belis J, Veer F, Lebet J. Durability of SG-laminated reinforced glass beams: Effects of temperature, thermal cycling, humidity and load-duration. Constr Build Mater 2012;27:280–92. https://doi.org/10.1016/j.conbuildmat.2011.07.046.

[19] Nhamoinesu S, Overend M. The mechanical performance of adhesives for a steel-glass composite façade system. Challenging Glas. 3 Conf. Archit. Struct. Appl. Glas. CGC 2012, Delft, Netherlands: 2012, p. 293–306. https://doi.org/10.3233/978-1-61499-061-1-293.

[20] Speranzini E, Agnetti S, Corradi M. Experimental analysis of adhesion phenomena in fibre-reinforced glass structures. Compos Part B Eng 2016;101:155–66. https://doi.org/10.1016/j.compositesb.2016.06.074.

[21] Bedon C, Machalická K, Eliášová M, Vokáč M. Numerical modelling of adhesive connections including cohesive damage. Challenging Glas. 6 Conf. Archit. Struct. Appl. Glas. CGC 2018 - Proc., 2018, p. 309–20. https://doi.org/10.7480/cgc.6.2155.

[22] Speranzini E, Agnetti S. The technique of digital image correlation to identify defects in glass structures. Struct Control Heal Monit 2014:1015–1029. https://doi.org/10.1002/stc.

[23] GOM. Correlate Software and Online Documentation. Rev.121188. 2019.

[24] Simulia. ABAQUS computer software and Online Documentation. v6.12. 2012.

[25] ISO. Plastics - Determination of tensile properties - Part 5: Test conditions for unidirectional fibre-reinforced plastic composites. 527-5, Genève, Switzerland: International Organization for Standardization; 2009, p. 11.

[26] SIKA. Technical Data Sheet SikaForce ® -7710 L100. 2008.

[27] SIKA. Technical Data Sheet Sikadur®-330. 2017.

[28] 3M. Technical Data Sheet 3M™ Scotch-Weld™ EPX™ Epoxy Adhesive DP490. 1996.

[29] ISO. Plastics – Determination of tensile properties – Part 2: Test conditions for moulding and extrusion plastics. 527-2, Genève, Switzerland: International Organization for Standardization; 2012, p. 5.

[30] ISO. Plastics – Determination of tensile properties – Part 1: General principles. 527-1, Genève, Switzerland: International Organization for Standardization; 2006, p. 13.

[31] ISO. Glass in building — Determination of the bending strength of glass — Part 3: Test with specimen supported at two points (four point bending). 1288-3, Genève, Switzerland: International Organization for Standardization; 2016.

[32] Machalická K, Vokáč M, Kostelecká M, Eliášová M. Structural behavior of double-lap shear adhesive joints with metal substrates under humid conditions. Int J Mech Mater Des 2019;15:61–76. https://doi.org/10.1007/s10999-018-9404-y.

[33] Belis J, Van Hulle A, Out B, Bos F, Callewaert D, Poulis H. Broad screening of adhesives for glass-metal bonds. Proc. Glas. Perform. Days 2011, Tampere, Finlandia: 2011, p. 286–9.

[34] Omairey S, Jayasree N, Kazilas M. Defects and uncertainties of adhesively bonded composite joints. SN Appl Sci 2021;3. https://doi.org/10.1007/s42452-021-04753-8.

[35] Feldmann M, Kasper R. Guidance for European Structural Design of Glass Components. Luxembourg: 2014. https://doi.org/10.2788/5523.

[36] Rodrigues A. Caracterização do comportamento do adesivo estrutural SikaForce 7710. Universidade de Coimbra, 2017.

[37] Haghani R, Al-Emrani M. A new design model for adhesive joints used to bond FRP laminates to steel

beams: Part B: Experimental verification. Constr Build Mater 2012;30:686–94. https://doi.org/10.1016/j.conbuildmat.2011.12.005.

[38] Sena-Cruz J. Strengthening of concrete structures with near-surface mounted CFRP laminate strips. Minho University, 2005.

[39] Focacci F, Nanni A, Bakis CE. Local Bond-Slip Relationship for FRP Reinforcement in Concrete. J Compos Constr 2000;4(1):24–31.

[40] Russo G, Zingone G, Romano F. Analytical Solution for Bond-SLip of Reinforcing Bars in R. C. Joints. J Struct Eng 1990;116:336–55.

[41] Sena-Cruz J, Barros J. Modeling of bond between near-surface mounted CFRP laminate strips and concrete. Comput Struct 2004;82:1513–21. https://doi.org/10.1016/j.compstruc.2004.03.047.

[42] Cunha V, Barros J, Sena-cruz J. Pullout Behavior of Steel Fibers in Self-Compacting Concrete. J Mater Civ Eng 2010;22:1–9.

[43] Biscaia H, Chastre C, Silva M. Linear and nonlinear analysis of bond-slip models for interfaces between FRP composites and concrete. Compos Part B 2013;45:1554–68. https://doi.org/10.1016/j.compositesb.2012.08.011.

[44] Biscaia H, Chastre C, Viegas A. A new discrete method to model unidirectional FRP-to-parent material bonded joints subjected to mechanical loads. Compos Struct 2015;121:280–95. https://doi.org/10.1016/j.compstruct.2014.10.036.

[45] Fernandes P. Bond behaviour of NSM CFRP-concrete systems: durability and quality control. Universdidade do Minho, 2016.

[46] Ko H, Matthys S, Palmieri A, Sato Y. Development of a simplified bond stress – slip model for bonded FRP – concrete interfaces. Constr Build Mater 2014;68:142–57. https://doi.org/10.1016/j.conbuildmat.2014.06.037.

[47] Dimande A. Influência da Interface no Reforço à Flexão de Estruturas de Betão com Sistemas FRP. Universidade do Porto, 2003.

LIST OF TABLES

Table 1. Main characteristics of the three adhesives used in this study according to their technical data sheets.

	Adhesives		
	SikaForce®-7710 L100 [26]	**SikaDur®-330** [27]	**3M DP490** [28]
Resin type	Polyurethane	Epoxy	Epoxy
Application	Adhesive for producing sandwich panels with low density materials (e.g. polyurethane foam) enclosed by structural materials (e.g. GFRP)	Adhesive for bonding CFRP materials to different substrates (e.g. concrete and glass)	Gap-filling adhesive for assembling different materials (e.g. CFRP and glass)
Curing time	21 days (+23 ºC / 50 % RH)	7 days (+23 ºC / 50 % RH)	7 days (+23 ºC / 50 % RH)
Shear strength	9.0 MPa 1)	> 4.0 MPa 2)	30.2 MPa 1)
Tensile strength	13.0 MPa	30 MPa	-
Service temperature	-	-40 ºC to +45 ºC	-80 ºC to +120 ºC
Viscosity	10000 mPas	6000 mPas	90000 mPas
Colour	Beige	Light grey	Black

1) Values determined from tensile tests on aluminium-to-aluminium single-lap joints – failure mode: cohesive failure in the adhesive
2) Value determined from pull-off tests on adhesive-concrete joints – failure mode: concrete fracture on the sandblasted substrate
Note: all mechanical properties shown were determined after the adhesive curing.

Table 2. Average values of the mechanical properties obtained for the involved materials: modulus of elasticity (E), tensile strength (σ_{ult}), yield strain (ε_y) and ultimate strain (ε_{ult}), along with the respective coefficient of variations (COV) in parenthesis.

Material	E [MPa]	σ_{ult} [MPa]	ε_y [‰]	ε_{ult} [‰]
Annealed glass	74000.0 (2.6%)	--	--	--
CFRP laminate	165200 (3.4%)	2418 (1.5%)	--	14.6 (2.5%)
SikaDur	4325.3 (3.1%)	32.34 (3.9%)	--	8.4 (5.4%)
SikaForce	48.4 (1.3%)	6.13 (1.7%)	205.6 (5.4%)	250.5 (7.7%)
3M	1728.1 (3.3%)	32.8 (4.2%)	--	30.7 (2.8%)

Table 3. Main tensile test results of double-lap joints with SikaDur, SikaForce and 3M adhesives, indicating in parentheses the coefficient of variation (COV) for each series. The following failure modes were identified: C-G, cohesive failure in glass when its tensile failure was achieved; I-AG, for adhesive failure by debonding at the interface adhesive/glass; FT-L, for fibre-tear failure in CFRP laminate; and CS-G, for cohesive shear debonding in glass.

	K [kN/mm]	F_{max} [kN]	d_{max} [mm]	Failure mode
SF-L25-I	109.70	18.2	0.39	I-AG
SF-L25-II	101.40	18.9	0.46	I-AG
SF-L25-III	98.70	17.0	0.37	I-AG
SF-L25-IV	100.40	14.3	0.38	I-AG
SF-L25	**102.6 (4.1%)**	**17.1 (10.4%)**	**0.40 (8.8%)**	-
SF-L50-I	162.89	23.44	0.17	C-G
SF-L50-II	157.55	31.17	0.25	C-G
SF-L50-III	146.17	22.97	0.18	C-G
SF-L50-IV	143.52	28.45	0.32	C-G
SF-L50	**152.5 (5.2%)**	**26.5 (13.0%)**	**0.23 (25.2%)**	--
SD-L25-I	452.3	19.6	0.046	FT-L + CS-G
SD-L25-II	486.4	25.1	0.055	FT-L + CS-G
SD-L25-III	483.7	24.2	0.054	C-G
SD-L25-IV	451.7	14.3	0.037	C-G
SD-L25	**468.5 (3.7%)**	**23.0 (10.5%)**	**0.048 (15.3%)**	--
SD-L50-I	599.1	22.1	0.051	FT-L + CS-G
SD-L50-II	533.8	24.5	0.049	FT-L + CS-G
SD-L50-III	543.9	20.1	0.060	FT-L + CS-G
SD-L50	**558.9 (5.1%)**	**22.2 (7.9%)**	**0.054 (8.9%)**	--
3M-L25-I	564.4	26.9	0.0531	C-G
3M-L25-II	502.2	28.8	0.067	C-G
3M-L25-III	544.8	29.3	0.060	C-G
3M-L25	**523.5 (4.9%)**	**28.4 (3.6%)**	**0.060 (9.4%)**	--
3M-L50-I	639.2	32.6	0.055	C-G
3M-L50-II	549.7	30.9	0.058	C-G
3M -L50-III	599.8	31.7	0.054	C-G
3M-L50	**596.2 (6.1%)**	**31.7 (2.2%)**	**0.056 (2.7%)**	--

Table 4. Comparison between the longitudinal strains induced by the lateral deflection of glass sheets in SF-L25-I, as measured using the strain gauges and the DIC (percentage difference in parenthesis).

	ε_{exp} [‰]	DIC method – Lateral bending		
		ε_{lin} [‰]	ε_{incr} [‰]	$\varepsilon_{lin} + \varepsilon_{incr}$ [‰]
SG1	0.127	0.205	-0.077	0.128 (1.2%)
SG2	0.076	0.208	-0.134	0.075 (-2.1%)

Table 5. Values of the parameters defining the $\tau - s$ relationship for each series of specimens with an overlap length of 25 mm.

	s_m **[mm]**	τ_m **[MPa]**	***Err*** **[%]**	$K_{a,s}$ **[MPa/mm]**
SF-L25	0.368	7.4	1.4	--
SD-L25	--	--	--	317.5
3M-L25	0.117	19.6	2.1	--

Table 6. Values of the parameters defining the $\tau - s_{eff}$ relationship for each series of specimens with an overlap length of 25 mm.

	s_m **[mm]**	τ_m **[MPa]**	$K_{a,s}$ **[MPa/mm]**
SF-L25	0.280	7.4	--
SD-L25	--	--	412.12
3M-L25	0.088	19.6	--

LIST OF FIGURES

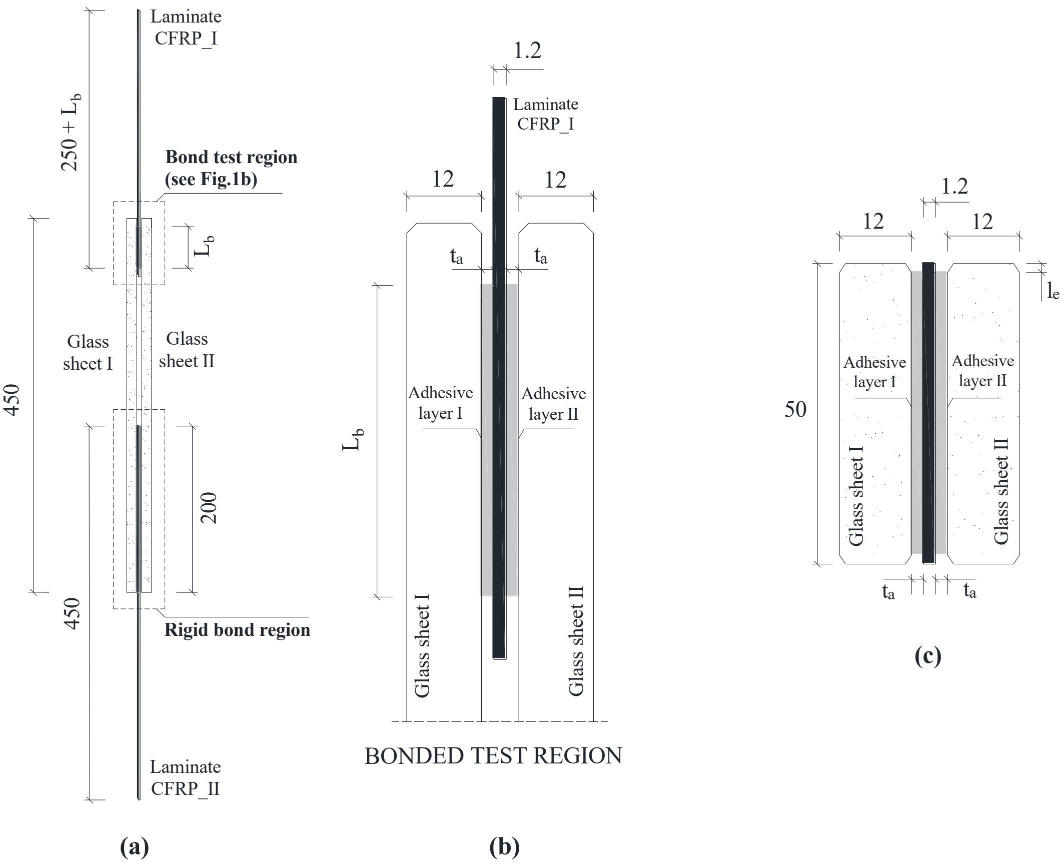

Fig. 1. Double-lap joint tests: (a) specimen's geometry, (b) studied connection and (c) connection cross-section. Units in [mm].

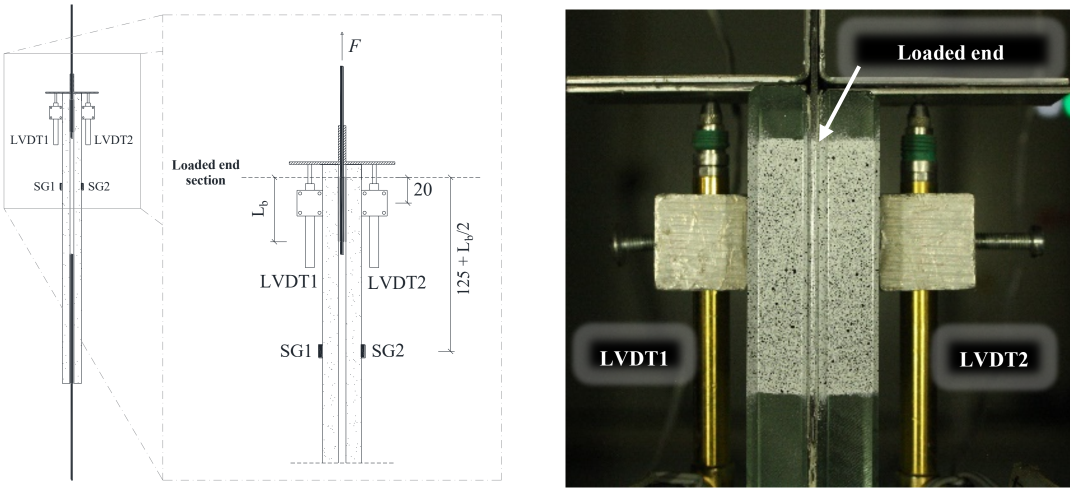

(a) **(b)**

878 **Fig. 2.** Double-lap joint tests: (a) schematic representation and (b) image showing the measuring systems adopted. Units in [mm].

879

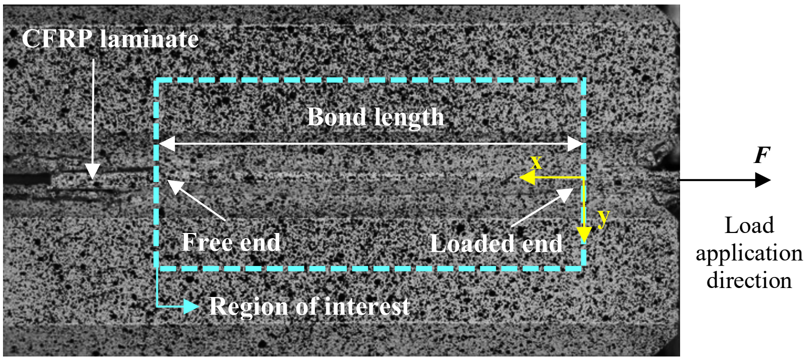

Fig. 3. Region of interest defined to the DIC analysis of the double-lap joints.

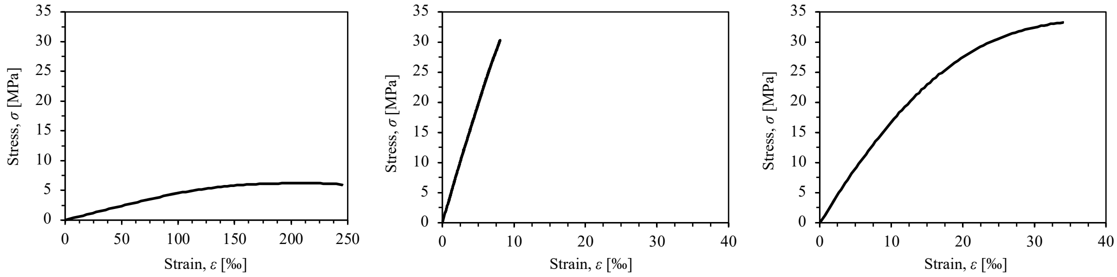

(a) **(b)** **(c)**

Fig. 4. Typical tensile stress-strain curves of the tested adhesives: (a) SikaForce; (b) SikaDur; and (c) 3M.

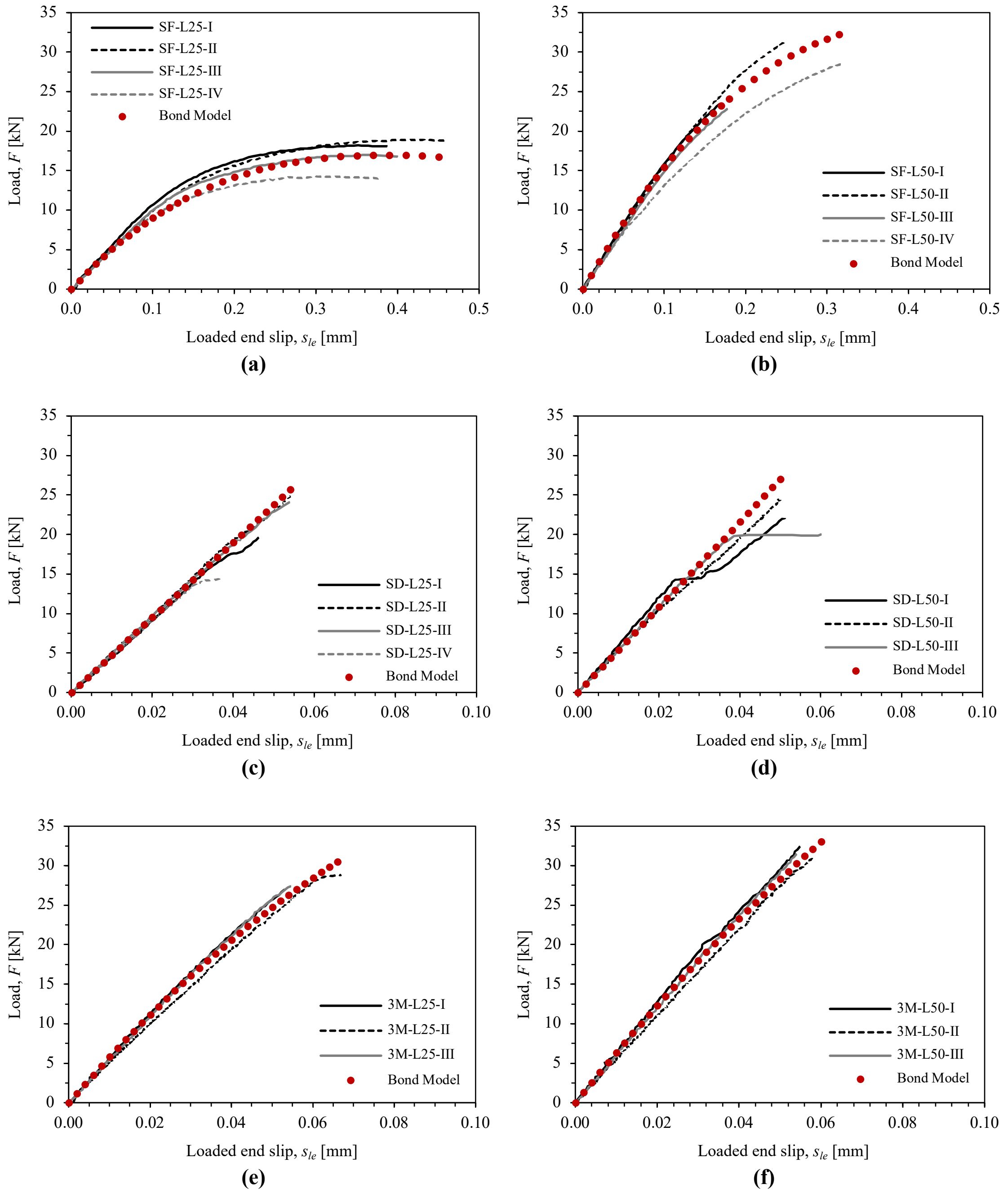

Fig. 5. Experimental and numerical load (F) *vs*. loaded end slip (s_{le}) responses obtained from the series of double-lap joints SF-L25 (a) and SF-L50 (b) with the SikaForce adhesive, SD-L25 (c) and SD-L50 (d) with the SikaDur adhesive, and 3M-L25 (e) and 3M-L50 (f) with the 3M adhesive. **Note:** 'Bond Model' is the analytical $F - s_{le}$ response obtained from the local $\tau - s$ laws calibrated in Section 4 for each type of adhesive.

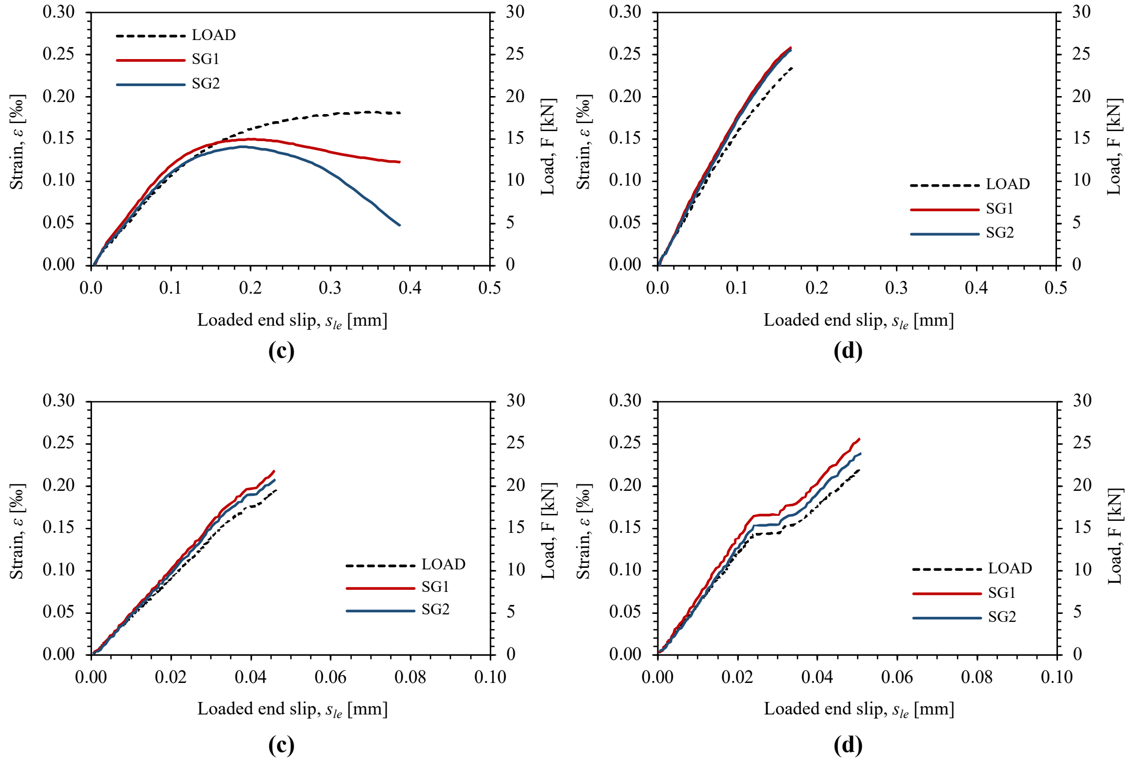

Fig. 6. Longitudinal strain in glass measured by strain gauges placed on the outer faces of both glass sheets, ε, and tensile load, *F*, *versus* the loaded end slip, s_{le}, for SF-L25-I (a), SF-L50-I (b), SD-L25-I (c) and SD-L50-I (d).

Adhesive	**Bond length**	
	L25	L50
SikaForce	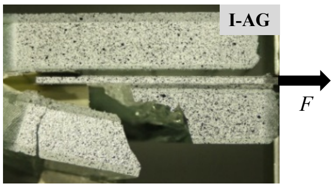	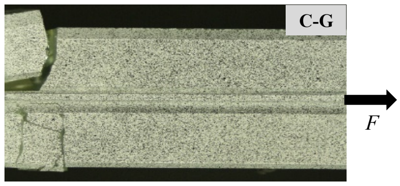
SikaDur	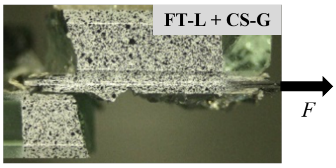	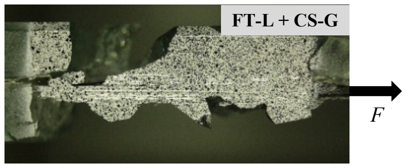
3M	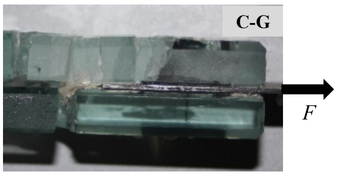	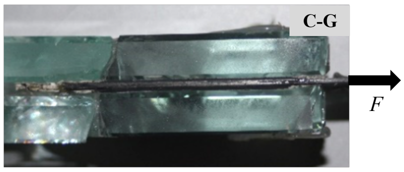

Fig. 7. Bond test region after collapse of double-lap joints, indicating the typical failure modes observed in each series, as well as the direction of load application.

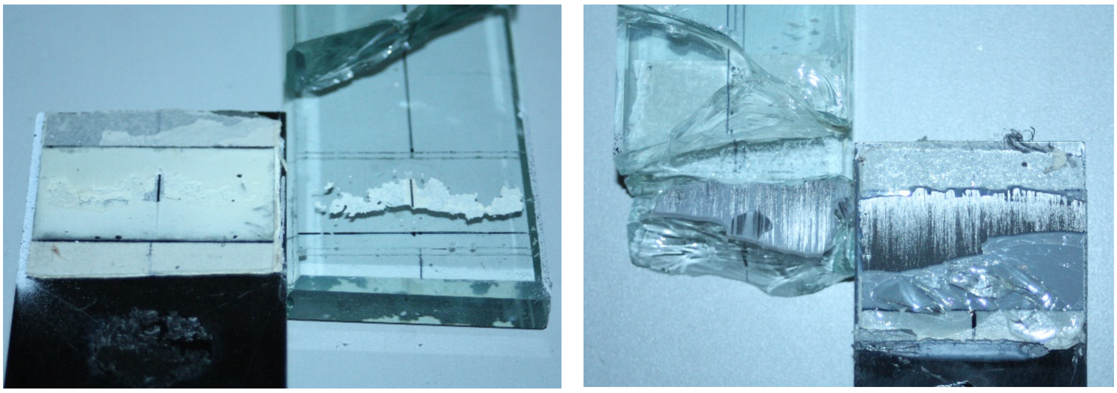

(a) **(b)**

Fig. 8. Debonding at the glass/adhesive interface in SF-L25 specimens (a) and cohesive shear debonding in adherends in SD-L25 specimens (b). In each case both images show the two opposite faces of the bonded connection after failure.

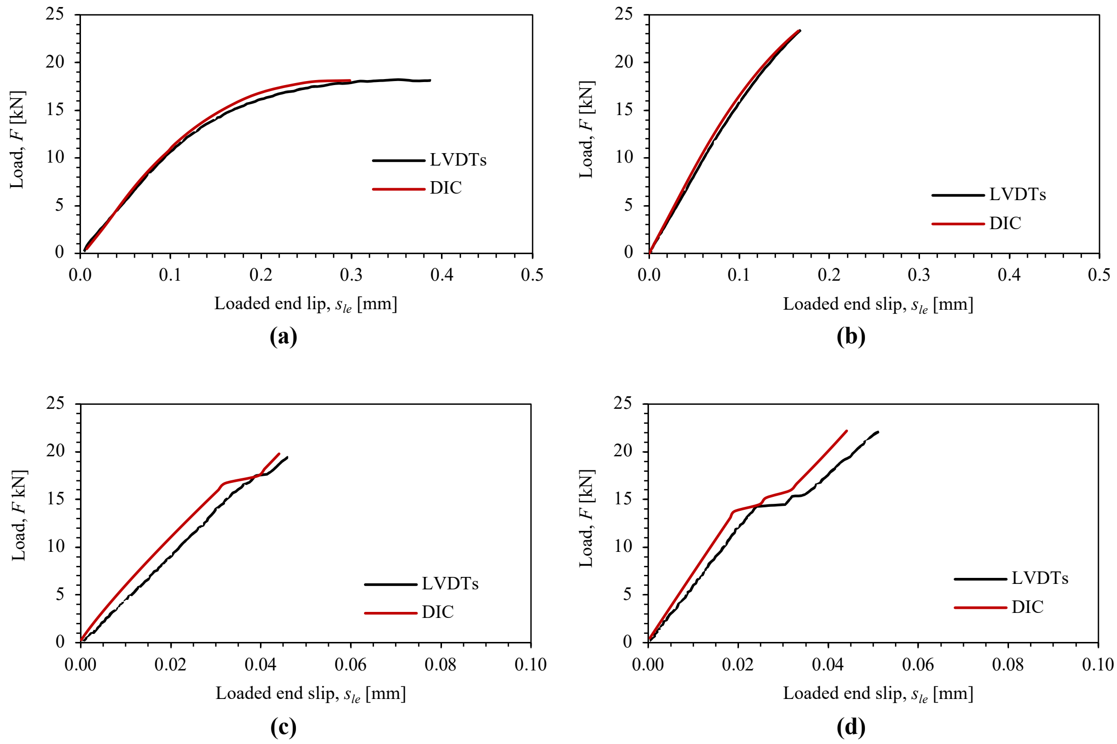

Fig. 9. Comparison between F - s_{le} curves extracted from the LVDTs and the DIC technique for (a) SF-L25-I, (b) SF-L50-I, (c) SD-L25-I and (d) SD-L50-I.

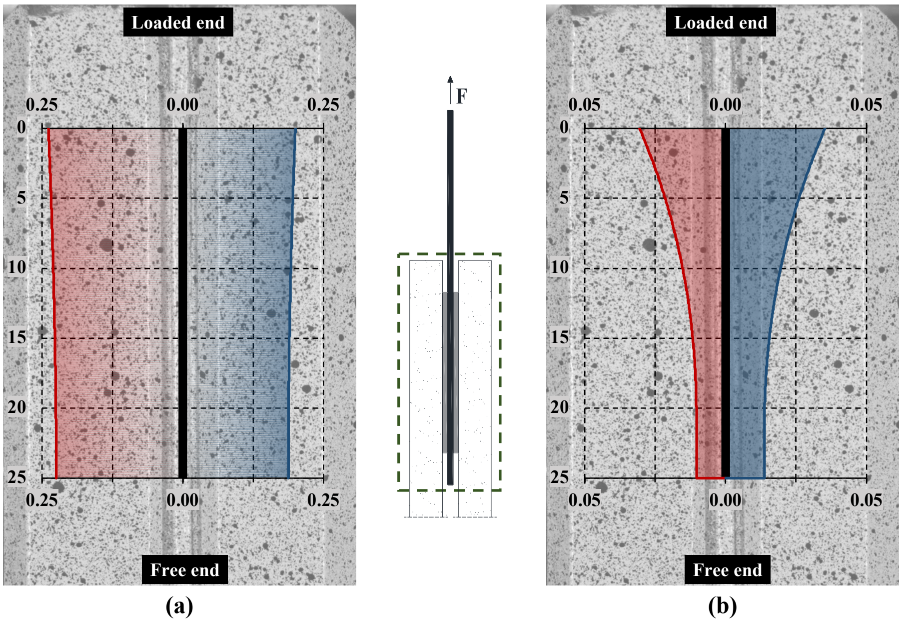

Fig. 10. Slip between the CFRP laminate and the glass sheets along L_b in SF-L25-I (a) and SD-L25-I (b), extracted from the DIC method for the last image captured before the failure. Note: all values in millimetres.

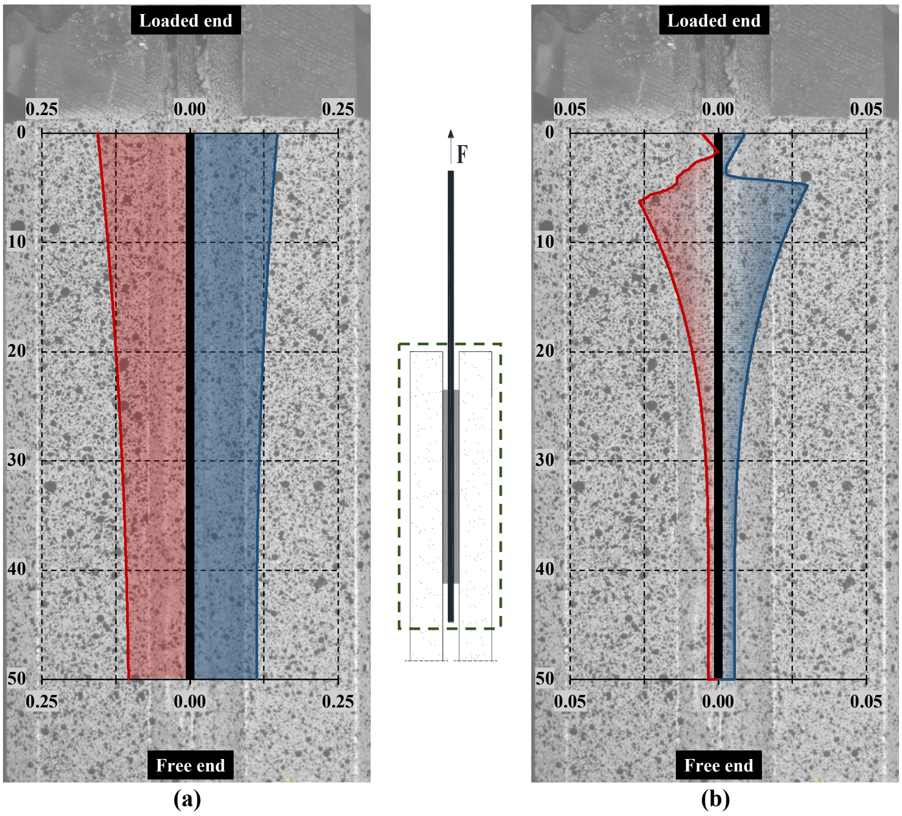

904 **Fig. 11.** Slip between the CFRP laminate and the glass sheets along L_b in SF-L50-I (a) and SD-L50-I (b), extracted from the DIC method for
905 the last image captured before the failure. Note: all values in millimetres.

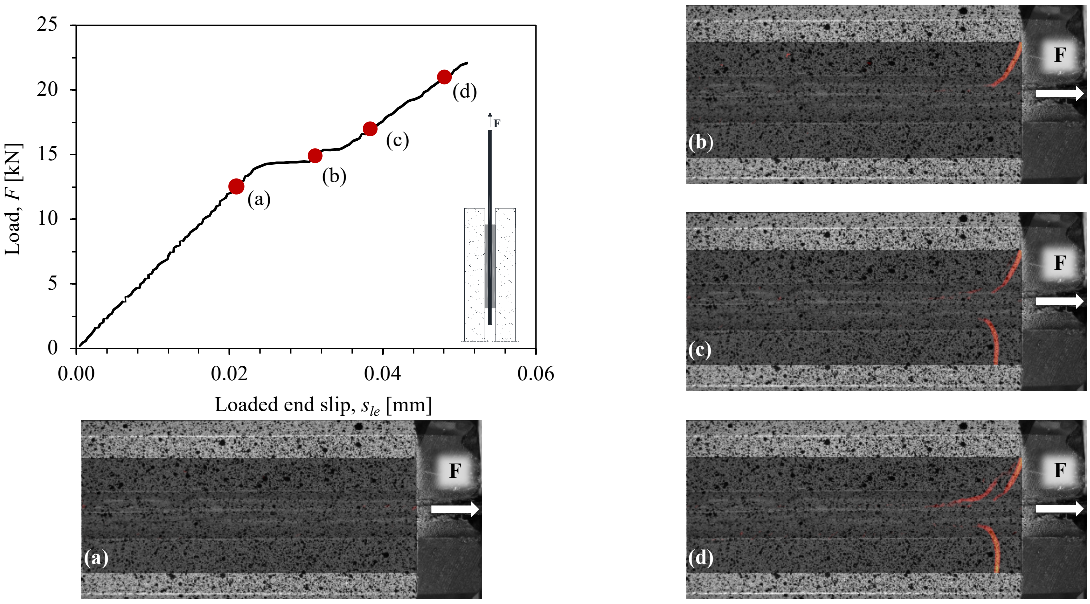

907 **Fig. 12.** Load (F) *vs*. slip (s_{le}) response obtained for the SD-L50-I specimen, together with the maximum principal strain fields obtained with
908 DIC at the ROI, showing the cracks formed at stages (a), (b), (c) and (d).

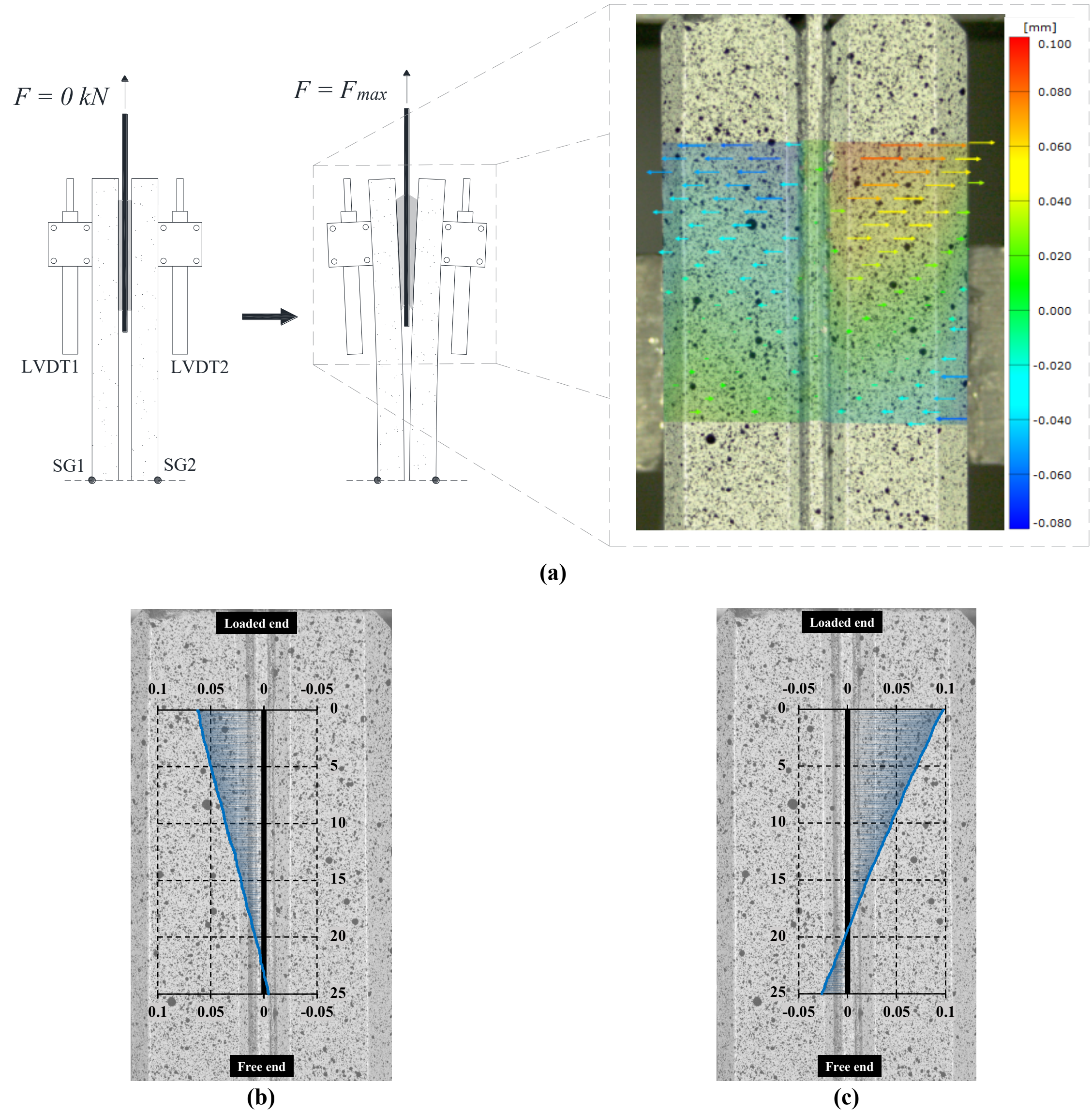

Fig. 13. Cleavage effect in SF-L25-I (a) showing the lateral deflection of the glass sheet I (b) and in the glass sheet II (c) in relation to the CFRP laminate. Note: nomenclature presented in Fig. 1 and all values in mm.

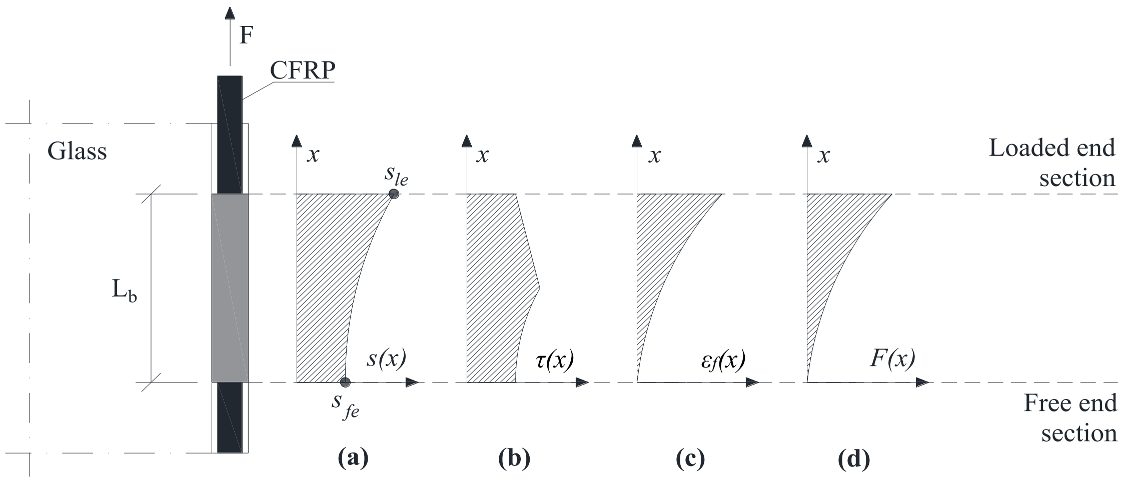

Fig. 14. Parameters involved in the analytical model [41]: (a) slip; (b) bond stress; (c) CFRP strain and (d) CFRP axial force.

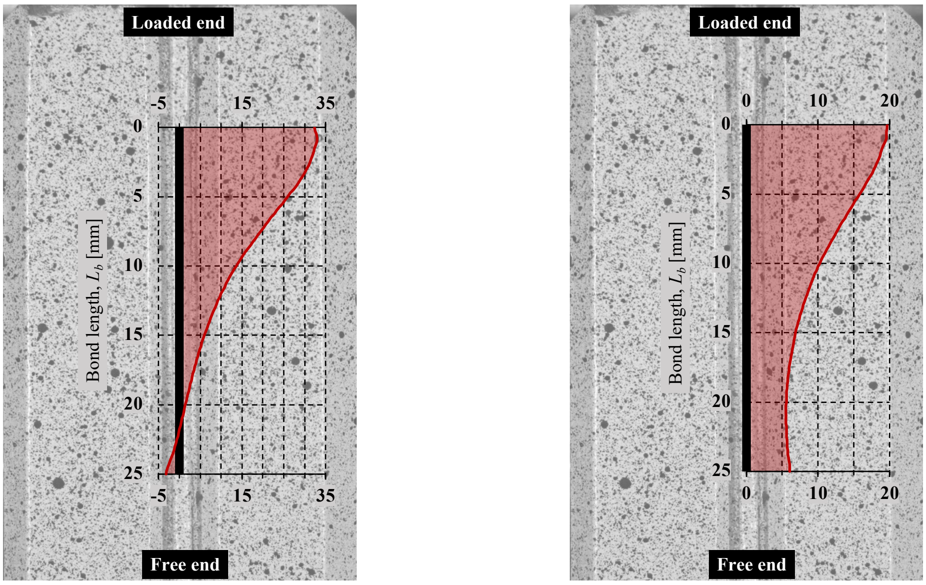

(a) (b)

Fig. 15. Distribution of maximum principal stress (a) and shear stress (b) along the bond length obtained for the 3M adhesive from numerical simulations, at the instant when the tensile strength of the 3M adhesive at the loaded end section was reached and the adhesive failure was initiated. Note: values of stress in MPa.

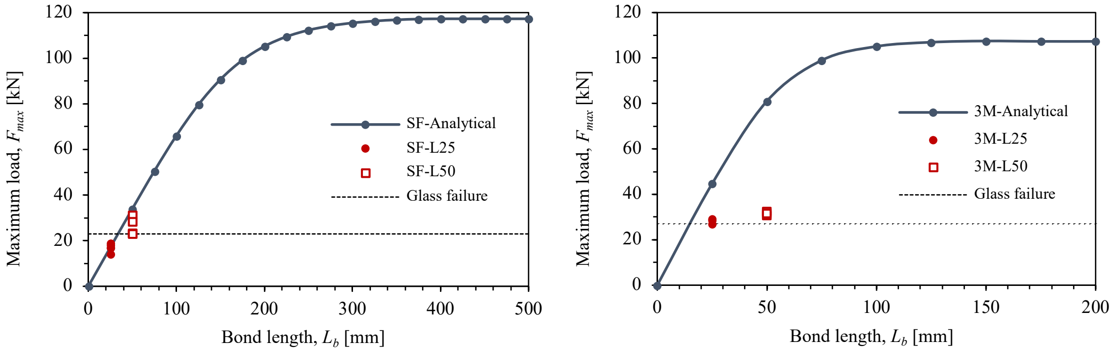

(a) **(b)**

Fig. 16. Comparison of the experimentally obtained Maximum load (F_{max}) for each bonded length (L_b) with the expected one using the analytical model for Sika Force (a) and 3M (b) adhesives.

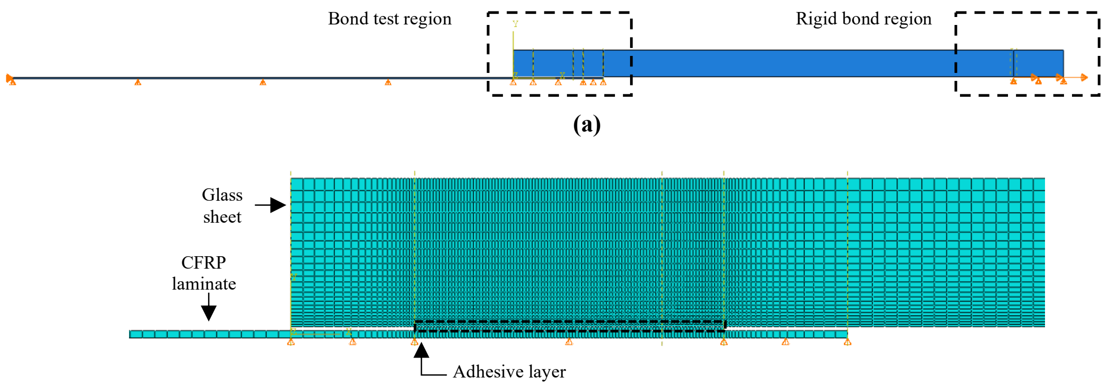

(b)

Fig. 17. Geometry, boundary conditions and load configuration used in the numerical simulation of the behaviour of double-lap joints (a), and detail of the bond test region showing the studied connection including the mesh and the boundary conditions(b).

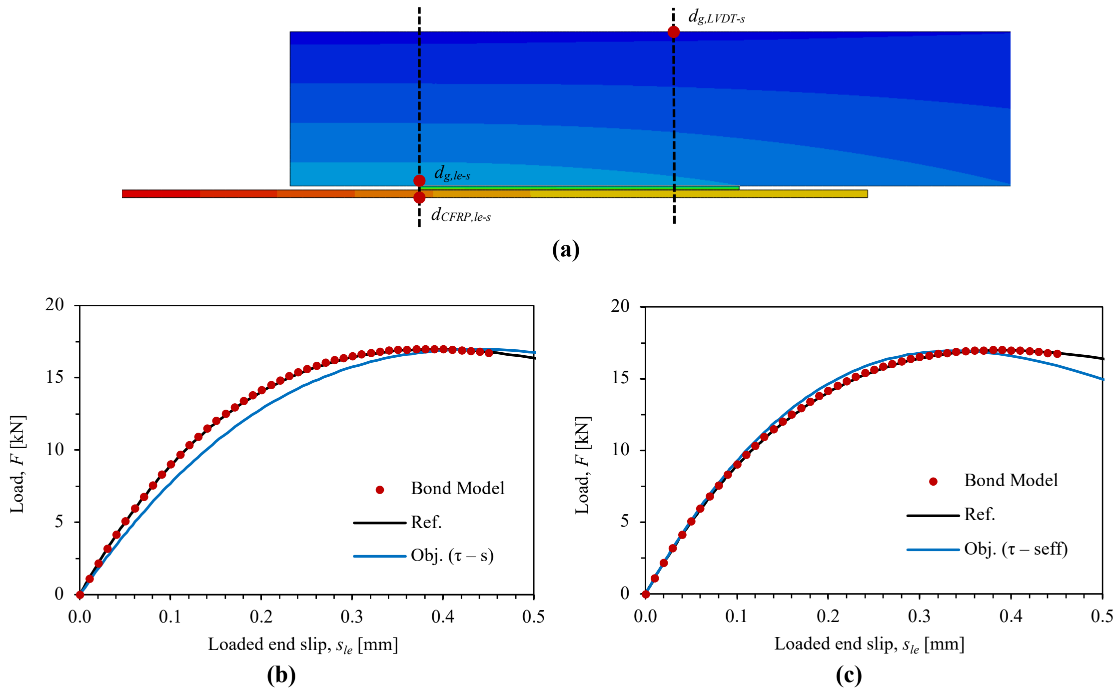

Fig. 18. Numerical model used in the iterative procedure applied to the SF-L25 series, showing the points where the displacements were measured (a) for the initial $\tau - s$ relationship (b) and for the numerically fitted $\tau - s_{eff}$ law.

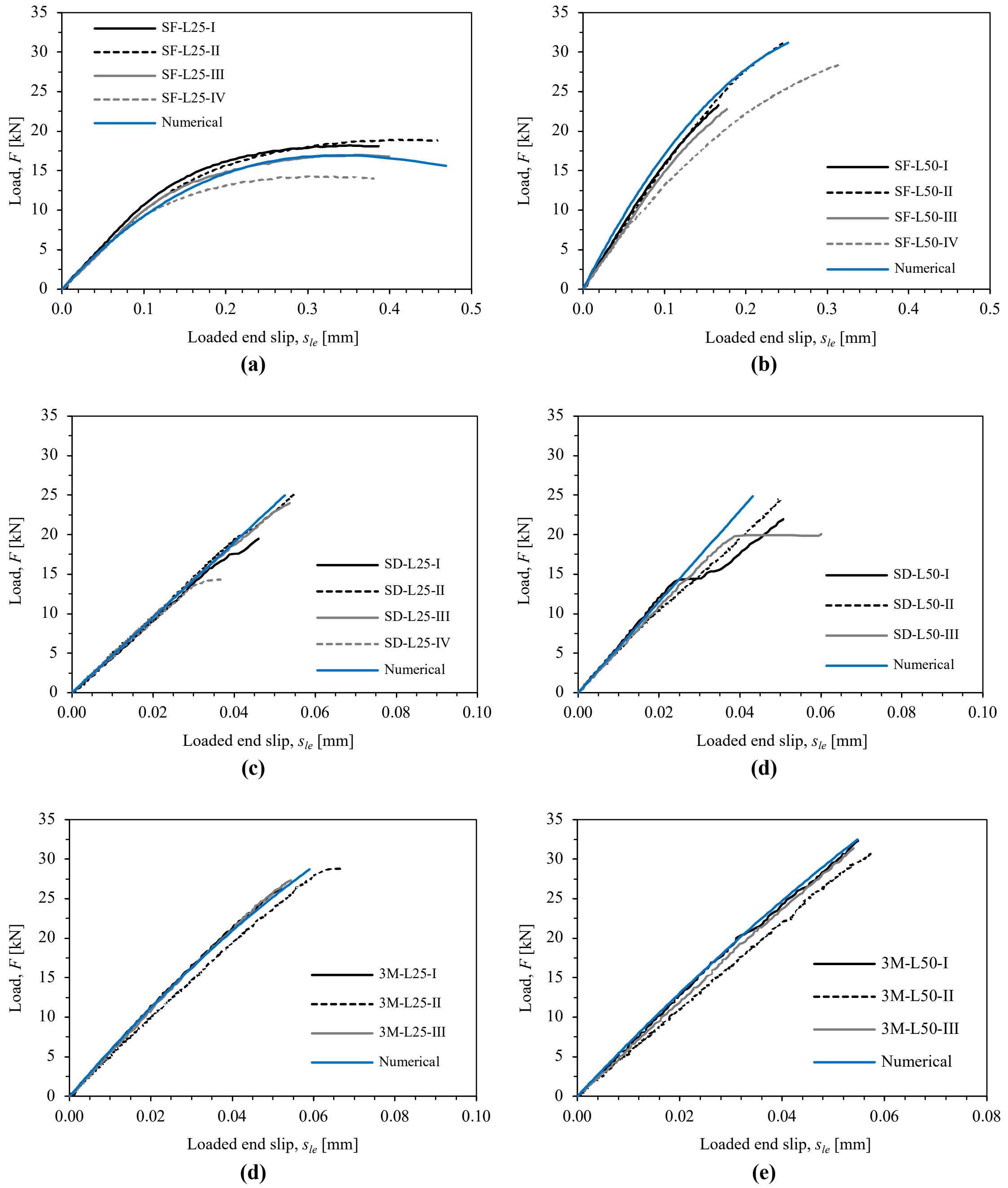

Fig. 19. Numerical and experimental load (*F*) *vs.* free end slip (s_{le}) responses for each series of double-lap joints: SF-L25 (a), SF-L50 (b), SD-L25 (c), SD-L50 (d), 3M-L25 (e) and 3M-L50 (f).

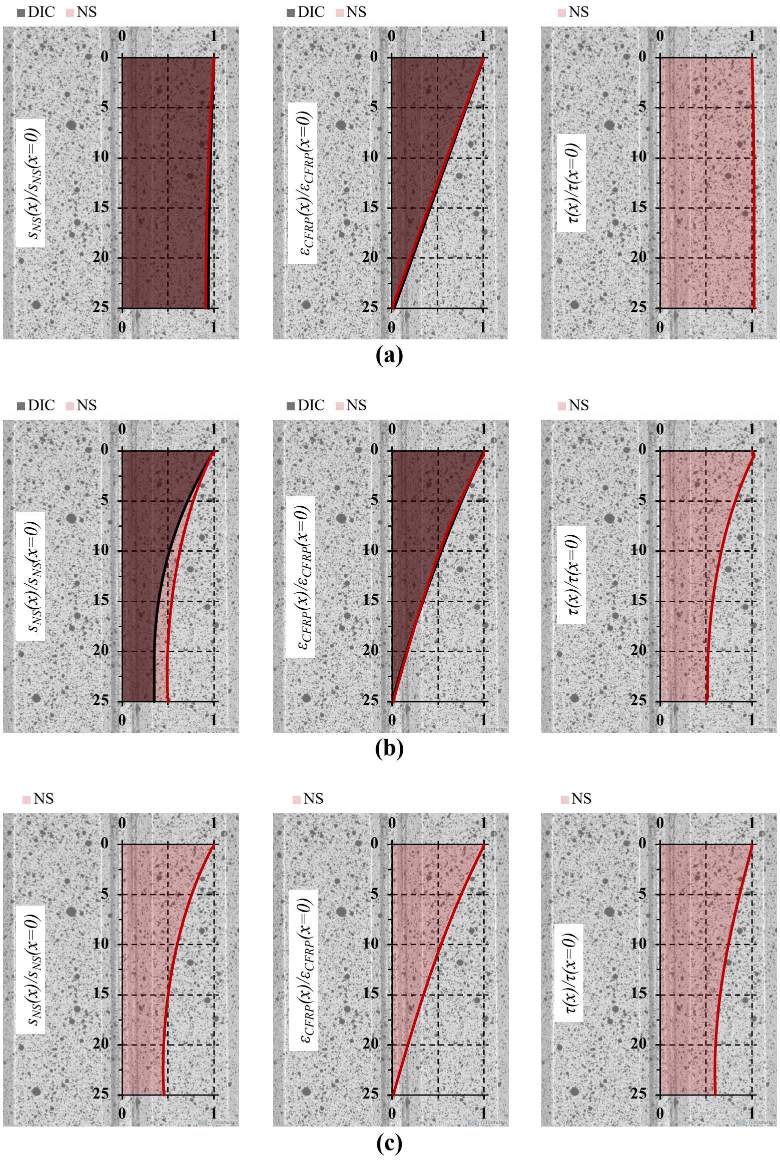

Fig. 20. Distribution of slip, CFRP strain and bond stress along the bond length obtained from DIC method (DIC) and numerical simulations (NS) for SF-L25-I (a), SD-L25-I (b) and 3M-L25-I (c) specimens. Note: values extracted when the maximum load was reached in each of the specimens.

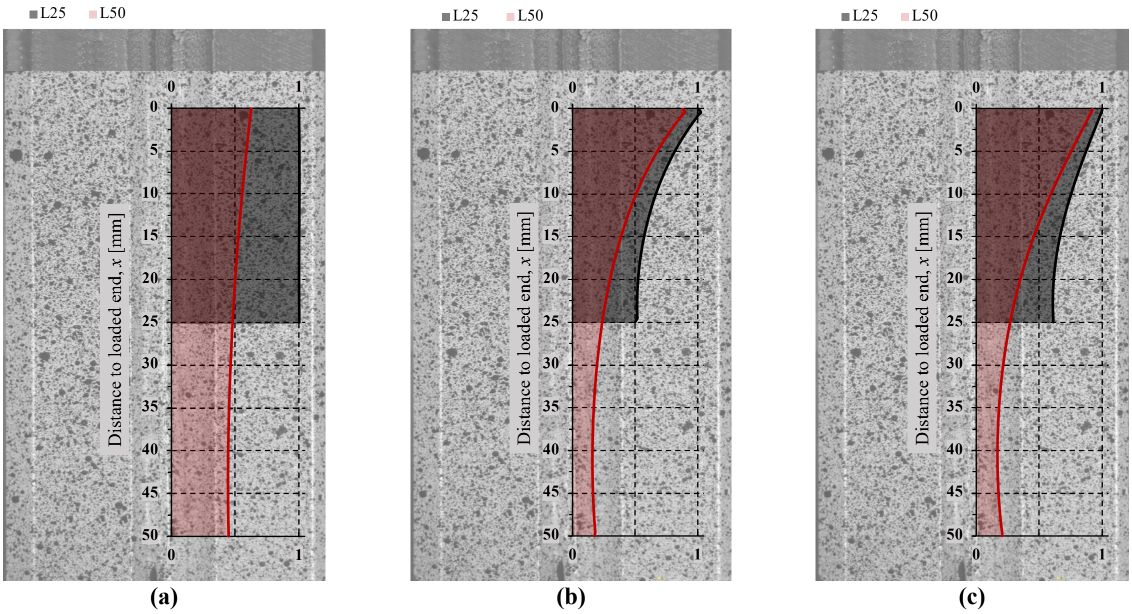

Fig. 21. Evolution of shear stress to shear strength ratio (horizontal axis) at different distances to the loaded end (vertical axis) along the ligament for both bond lengths of each adhesive: SF (a), SD (b) and 3M (c) specimens. Note: values extracted from the numerical models for the average maximum load of the corresponding L25 series.